

The molybdenum isotopic compositions of I-, S- and A-type granitic suites

Jie Yang^{a,b,*}, Jane Barling^b, Christopher Siebert^c, Jan Fietzke^c, Ed Stephens^a,
Alex N. Halliday^b

^a Department of Earth & Environmental Sciences, University of St Andrews, Fife KY16 9AL, UK

^b Department of Earth Sciences, University of Oxford, South Parks Road, OX1 3AN, UK

^c GEOMAR, Helmholtz Centre for Ocean Research Kiel, Wischhofstraße 1-3, D-24148 Kiel, Germany

Received 24 October 2015; accepted in revised form 12 January 2017; Available online 30 January 2017

Abstract

This study reports Mo isotopic compositions for fifty-two Palaeozoic granitic rocks with contrasting source affinities (A-, I- and S-type) from the Lachlan Fold Belt (LFB) and the New England Batholith (NEB), both in SE Australia, and three compositionally zoned plutons (Loch Doon, Criffell, and Fleet) located in the Southern Uplands of Scotland. The results show relatively large variations in $\delta^{98}\text{Mo}$ for igneous rocks ranging from -1.73‰ to 0.59‰ with significant overlaps between different types. No relationships between $\delta^{98}\text{Mo}$ and $\delta^{18}\text{O}$ or ASI (Alumina Saturation Index) are observed, indicating that Mo isotopes do not clearly distinguish igneous vs. sedimentary source types. Instead, effects of igneous processes, source mixing, regional geology, as well as hydrothermal activity control the Mo isotope compositions in these granites. It is found that Mo is mainly accommodated in biotite and to a lesser extent in hornblende. Hornblende and Fe^{3+} -rich minerals may preferentially incorporate light isotopes, as reflected by negative correlations between $\delta^{98}\text{Mo}$ and K/Rb and $[\text{Fe}_2\text{O}_3]$. There is a positive correlation between initial $^{87}\text{Sr}/^{86}\text{Sr}$ and $\delta^{98}\text{Mo}$ in I-type granitic rocks, reflecting the admixing of material from isotopically distinct sources. Granitic rocks from Scotland and Australia display strikingly similar curvilinear trends in $\delta^{98}\text{Mo}$ vs. initial $^{87}\text{Sr}/^{86}\text{Sr}$ despite the differing regional geology. Localized hydrothermal effects can result in low $\delta^{98}\text{Mo}$ in granite, as seen in three samples from Loch Doon and Criffell which have anomalously light $\delta^{98}\text{Mo}$ of $<-1\text{‰}$. Based on this study, an estimate of $\delta^{98}\text{Mo} = 0.14 \pm 0.07\text{‰}$ (95% s.e.) for the Phanerozoic upper crust is proposed. This is slightly heavier than basalts indicating an isotopically light lower crust and/or a systematic change to the crust resulting from subduction of isotopically light dehydrated slab and/or pelagic sediment over time.

© 2017 The Authors. Published by Elsevier Ltd. This is an open access article under the CC BY license (<http://creativecommons.org/licenses/by/4.0/>).

Keywords: Molybdenum isotopes; Granitic rock; Granite; A-type; I-type; S-type; Lachlan Fold Belt; Loch Doon; Criffell; Fleet; The upper crust

1. INTRODUCTION

Stable molybdenum (Mo) isotopes in marine sediments have been widely used for paleo-redox reconstruction (e.g.

Siebert et al., 2003; Planavsky et al., 2014) on the basis that significant isotopic fractionation occurs in low-temperature (low-T) settings, leading to isotopically distinct marine sediments depending on their redox conditions during formation (e.g. Barling et al., 2001; Siebert et al., 2003; Anbar, 2004; Tossell, 2005). Yet the continental baseline for Mo isotopes, which is essential to the application of this proxy, is still poorly constrained to date. The Mo isotopic

* Corresponding author at: School of Earth & Environmental Sciences, University of St Andrews, Fife KY16 9AL, UK.

E-mail address: jy42@st-andrews.ac.uk (J. Yang).

composition ($\delta^{98}\text{Mo}$) of the continental crust has long been uncertain. It was first approximated to be $\sim -0.25\text{‰}$ (all $\delta^{98}\text{Mo}$ values in this study were (re-) normalised to NIST SRM3134, i.e. the $\delta^{98}\text{Mo}$ composition of NIST SRM 3134 is set to 0‰) based on few analyses of molybdenites (Barling et al., 2001) and igneous rocks (Siebert et al., 2003). This value was later revised to be $\sim 0.4\text{‰}$ heavier based on high-temperature molybdenites (Greber et al., 2014) and arc lavas (Voegelin et al., 2014). However, these estimates are still limited by the fact that 1) the lithologies used are not fully representative of the composition of the continental crust and 2) the number of samples is too limited to make a constrained assessment. High temperature materials investigated so far for Mo isotope fractionation are komatiites (Greber et al., 2015), arc lavas (Siebert et al., 2003; Voegelin et al., 2014; Freymuth et al., 2015, 2016; König et al., 2016), an Icelandic lava sequence (Yang et al., 2015), molybdenite deposits (e.g. Wieser and de Laeter, 2003; Hannah et al., 2007; Mathur et al., 2010; Greber et al., 2011, 2014; Shafiei et al., 2014) and a few silicic rocks (Siebert et al., 2003; Voegelin et al., 2012; Greber et al., 2014). The rather small database and relatively poor understanding of the behaviour of Mo isotopes in high-temperature conditions, is in stark contrast to knowledge of Mo isotope behaviour at low-temperatures, and hinders constraint of the Mo isotopic composition of the continental crust. Granitic rocks, used in the broadest sense here to include plutonic rocks of intermediate to felsic compositions including granite more strictly as well as trondjemite, tonalite, granodiorite and diorite, are particularly poorly represented in the existing database but comprise a major part of the continental crust (Wedepohl, 1991). This work therefore focuses on granitic lithologies, and thus increases the database of continental Mo isotope data significantly.

Granitic magmas may in principle derive from one or more of the following processes:

- (1) fractional crystallization of primary basaltic melts
- (2) partial melting of subducted oceanic crust
- (3) partial melting of mantle-derived protoliths in the crust
- (4) anatexis of more evolved crustal lithologies including sediments

The significant Mo isotope fractionation under low-T conditions in the hydrosphere suggests that Mo isotopes in sediments must be significantly fractionated from igneous materials. A second objective of this study was therefore to test if the involvement of sediments in granite genesis can be traced using Mo isotopes. We test this possibility by investigating granitic rocks with a variety of known source affinities.

To constrain the budget and the behaviour of Mo isotopes in the continental crust, as well as to explore whether Mo isotopes can be a diagnostic indicator of granite provenance, we have investigated a large set of well-characterised granitoid samples derived from distinct sources, including A-, I- and S-type granitic rocks.

2. SAMPLES

Granitic rocks in the Australian Lachlan Fold Belt (LFB) are subdivided into I-type and S-type, based on the analysis of mineralogy and major element chemical composition (Chappell and White, 2001). I-type granites (igneous and intracrustal sources) are thought to be sourced from unexposed igneous precursors. They range in composition from felsic to intermediate, usually have high Na_2O and CaO contents and have ASI values < 1.1 (Alumina Saturation Index = molar $[\text{Al}_2\text{O}_3/(\text{CaO} + \text{Na}_2\text{O} + \text{K}_2\text{O})]$; Shand (1927)). S-type (sedimentary source) granites, derived by anatexis of sedimentary protoliths that have experienced at least one cycle of weathering, are mainly restricted to high SiO_2 compositions, and are characterised by relatively low concentrations of Na_2O and CaO , with high ASI values (> 1.1). Due to the contrasting contents of aluminum and alkalis, I-types are commonly hornblende- and sphene-bearing, whereas S-types are hornblende-absent, and may contain monazite. Mica and apatite can be found in both I- and S-types. A-type (alkaline, anhydrous, or anorogenic) granites, first defined by Loiselle and Wones (1979) are thought to have formed through fractional crystallization of basaltic magmas or partial melting of intermediate crustal basement at high temperature ($> 850^\circ\text{C}$). Relative to I- and S-types, A-type granites are characterised by high SiO_2 , FeO (total), alkali and halogen elements, and low MgO , Al_2O_3 , CaO , and H_2O contents (e.g. Whalen et al., 1987; Eby, 1990; Frost and Frost, 2010).

2.1. A-, I- and S-type granites, and sediments from SE Australia

Twenty plutonic and four sedimentary samples from well-characterised granitic outcrops of the LFB and New England Fold Belt (NEFB) in SE Australia were analysed in this study. The Lachlan and New England orogens are north–south trending deformed regions in SE Australia, which developed as parts of the eastern margin of Gondwanaland during the Cambrian–Devonian (Foster and Gray, 2000). Voluminous granitic plutons intruded into metasedimentary rocks in both the LFB and NEFB in response to convergent marginal tectonism during the Palaeozoic and early Mesozoic (Chappell and Simpson, 1984; Foster and Gray, 2000).

Although the LFB granites are divided into two contrasting categories (I-type and S-type) they display significant compositional overlap in their Nd and Sr isotopic compositions (e.g. McCulloch and Chappell, 1982; Keay et al., 1997) and trace element patterns (e.g. Collins, 1998). Therefore, rather than discrete sources, some authors have proposed models involving mixing of two or three distinct sources including a primitive depleted mantle component, Cambrian greenstones within the belt and the widespread Ordovician marine turbidites (Gray, 1984; Keay et al., 1997). The turbidites are also present as country rocks for the LFB intrusives (Wyborn and Chappell, 1983).

2.1.1. Bega and Moruya batholiths, LFB

Six I-type samples from three supersuites of the 425–389 Ma Bega batholith (five samples from Glenbog, Tonghi, and Brogo), and the 395–389 Ma Moruya batholith (one sample) were analysed. These plutons outcrop along the east margin of the LFB, with the majority being I-type granites (Chappell et al., 1991). The samples cover a range of 65–73 wt.% of SiO₂ content (Table 1). The Moruya sample has the most primitive radiogenic Sr and Nd isotopic composition of all the I- and S-type granites investigated.

2.1.2. Gabo and Mumbulla suites, LFB

Four A-type granites were studied, sampled from two A-type suites (Gabo and Mumbulla). These suites are adjacent to the eastern side of the Bega batholith, with the Gabo suite located in the south and the Mumbulla in the north. Gabo suite granites are thought to be Upper Devonian intrusions (e.g. Collins et al., 1982). One sample analysed was taken from one of the six identified plutons (Watergums) in Gabo. The Mumbulla suite comprises the Mumbulla and Dr. George plutons, and both intrude the Bega Batholith and Ordovician metasediment. Two samples from Mumbulla, and one from Dr. George were analysed. All the A-type granites are highly silicic (SiO₂ ≥ 74 wt.%), and can be distinguished from other granite types by higher abundances of large highly charged cations (e.g. Nb, Ga, Y) and REE but lower Al, Mg and Ca contents (Collins et al., 1982).

2.1.3. Berridale batholith, LFB

Eight samples were analysed from the Berridale Batholith (428–410 Ma), comprising three I-type and five S-type granites. The Berridale Batholith is located towards the centre of the LFB across the IS-line (White et al., 1976) and features approximately equal volumes of I- and S-type granitic bodies.

Five S-type granites were sampled from three identified S-type suites, the Cootralantra, Dalgety and Tingaringhy. These samples cover a limited range of SiO₂ contents (67–73 wt.%) (Chappell et al., 1991) and have εNd, ⁸⁷Sr/⁸⁶Sr and δ¹⁸O that match their inferred sedimentary sources.

The I-type granites of the Berridale Batholith have bimodal compositions characterised by felsic and relatively mafic plutons. Samples from both categories were chosen for analysis in this study, including one more mafic (Tara, 68 wt.% SiO₂) and two more felsic (Maffra and Buckley's Lake; 77 and 71 wt.% SiO₂, respectively).

Compared to the S-type samples (initial εNd = −8.4 to −6.1, initial ⁸⁷Sr/⁸⁶Sr = 0.710–0.712), I-type samples have much more primitive radiogenic isotopic compositions (initial εNd = −3.2 to +0.0, initial ⁸⁷Sr/⁸⁶Sr = 0.705–0.707). However, all the Berridale samples display heavy δ¹⁸O, with I-types (δ¹⁸O = 7.9‰–9.3‰) slightly lighter than S-types (δ¹⁸O = 9.2‰–10.5‰).

2.1.4. Wagga batholith, LFB

One S-type granite from the Wagga batholith (440–425 Ma) was analysed. The Wagga batholith is located towards the western margin of the LFB. This region is

dominated by S-type granites (Chappell et al., 1991), and may have the thickest meta-sedimentary stack (e.g. Collins, 1998). The Wagga sample shows evident S-type features, such as high ASI (1.3) and initial ⁸⁷Sr/⁸⁶Sr (0.716).

2.1.5. Ordovician turbidites, LFB

Four Ordovician turbidites from the Snowy Mountains, South-eastern Australia were analysed, including two silica-rich (detrital quartz) and two clay-rich (silica-poor) samples. Ordovician sedimentary rocks are widespread throughout the LFB. These materials are first described in detail by Wyborn and Chappell (1983) and considered to be the main sedimentary protolith for the S-type granites in the LFB (e.g. Keay et al., 1997).

2.1.6. New England Batholith, NEFB

We have analysed one S-type granite sample from one of the granitic suites of the New England Batholith (NEB), the Bundarra Plutonic suite (286 Ma), which is located in the south part of the New England Fold Belt (Leitch, 1974; Flood and Shaw, 1975). The Bundarra suite comprises a series of north–south trending plutonic bodies, which outcrops along the eastern margin of the NEB. This suite shows many classic features of S-type granites, such as high ASI values, cordierite-bearing mineralogy and significantly elevated δ¹⁸O (>10‰) (Shaw and Flood, 1981). However, the initial ⁸⁷Sr/⁸⁶Sr and εNd signatures of 0.705–0.706 and +0.8 to +2.3 respectively, are relatively primitive. Therefore, these S-types were proposed to have been derived from both felsic and mafic sedimentary components (Mensel et al., 1985).

2.2. Granitic rocks from Scotland

We have also studied well-characterised samples from 3 compositionally zoned plutons from the ~400 Ma Caledonian plutons of the Southern Uplands of Scotland. Thirty-two samples, with SiO₂ ranging from 59.1 to 75.7 wt.%, from the three largest plutons (Loch Doon, Criffell and Fleet) were selected for analysis. These plutons show well defined features of inward zoning to more evolved chemical compositions accompanied by an overall increase in initial ⁸⁷Sr/⁸⁶Sr and δ¹⁸O. The isotopic variations suggest the emplacement of these plutons involved basaltic/andesitic and metasediment-derived components (Halliday et al., 1980; Stephens and Halliday, 1980; Holden et al., 1987). The overall contribution of sedimentary protolith to the magmas increases from Loch Doon to Criffell to Fleet. Detailed mineralogical, chemical and field characteristics are described in Halliday et al. (1980).

2.2.1. Loch Doon

The Loch Doon pluton (408 Ma) displays the greatest petrological variation in an approximately concentric pattern including diorite, monzodiorite, granodiorite and granite from the margins inwards (Gardiner and Reynolds, 1932; Tindle and Pearce, 1981). The compositional zoning structure of the Loch Doon pluton was interpreted to have formed as a result of pulses of successive magmas from differing sources accompanied by fractional crystallization

Table 1

Molybdenum isotope and concentration data for granites and sediments from Australia analysed in this study. Mo isotopic composition ($\delta^{98}\text{Mo}$) is relative to NIST SRM3134. Each $\delta^{98}\text{Mo}$ value represents the average of two to four full procedural duplicates and the reproducibilities of all samples are better than ± 0.06 (2 s.d.). Silicon isotope data are taken from [Savage et al. \(2012\)](#). Other data are taken from the following sources: LFB: [Collins et al. \(1982\)](#), [Chappell et al. \(1991\)](#); [Gray \(1990\)](#); [McCulloch and Woodhead \(1993\)](#); [O'Neil and Chappell \(1977\)](#); [Wyborn and Chappell \(1983\)](#); NEB: [O'Neil et al. \(1977\)](#); [Mensel et al. \(1985\)](#), [Shaw and Flood \(1981\)](#).

Sample	Type	Locality	$\delta^{98}\text{Mo}$ ‰	$\delta^{30}\text{Si}$ ‰	$\delta^{18}\text{O}$ ‰	$^{87}\text{Sr}/^{86}\text{Sr}(\text{i})$	SiO_2 wt. %	TiO_2 wt. %	Fe_2O_3 wt. %	FeO wt. %	K_2O wt. %	Mo $\mu\text{g/g}$	Rb $\mu\text{g/g}$	ASI
Lachlan Fold Belt														
<i>Gabo suite</i>														
GI1	A-type	Watergums	−0.15				73.6	0.34	1.42	1.49	4.23	2.4	210	0.98
<i>Mumbulla suite</i>														
AB113	A-type	Dr. George	−0.10				77.0	0.12	0.14	1.14	5.16	2.0	240	1.08
AB117	A-type	Mumbulla	0.04				77.0	0.15	0.40	1.05	4.98	1.8	230	1.03
AB202	A-type	Mumbulla	0.59					0.12	0.34	0.89	4.87	8.1	242	1.05
<i>Bega</i>														
AB006	I-type	Glenbog	0.16	−0.18	8.80	0.70869	67.4	0.53	1.58	3.02	2.99	0.6	135	0.95
AB102	I-type	Glenbog	0.32	−0.18		0.70790	72.2	0.39	0.49	2.34	3.52	0.7	164	1.02
AB195	I-type	Glenbog	−0.02	−0.19	9.20	0.70544	65.3	0.58	1.76	2.83	3.43	1.6	133	0.94
AB234	I-type	Tonghi	0.23	−0.24		0.70869	69.2	0.41	1.05	2.62	3.60	1.0	163	0.98
AB82	I-type	Brogo	0.02	−0.21		0.70456	67.2	0.47	1.44	2.05	2.66	0.5	92	0.96
<i>Moruya</i>														
MG58	I-type		−0.35	−0.14	8.10	0.70410	72.5	0.31	2.63		2.54	0.1	60	1.1
<i>Berridale</i>														
BB10	I-type	Buckleys Lake	0.17	−0.18	8.78	0.70673	71.2	0.37	1.18	1.40	3.98	1.2	190	1.00
BB21	I-type	Maffra	0.13	−0.15	9.32	0.70504	76.6	0.19	0.43	0.43	4.16	0.4	214	1.05
BB87	I-type	Tara	−0.07	−0.25	7.86	0.70628	67.7	0.47	1.45	2.36	2.31	0.5	84	0.97
BB09	S-type		0.16	−0.26	9.56	0.70986	68.2	0.53	0.93	3.10	3.77	0.5	179	1.08
BB12	S-type		0.15	−0.25	9.2	0.70991	66.9	0.55	0.83	3.47	3.48	1.3	173	1.06
BB53	S-type		0.18	−0.33	10.53	0.71153	67.4	0.53	0.71	3.60	3.41	0.6	164	1.13
BB83	S-type		0.14	−0.22	10.55	0.71206	67.4	0.53	1.58	3.02	2.99	0.7	135	1.16
BB02	S-type		−0.04	−0.23	10.23	0.71076	73.5	0.22	0.44	1.47	4.63	4.3	236	1.09
<i>Waga</i>														
VB140	S-type	Granya	0.16	−0.40		0.71580	72.5	0.25	0.29	1.33	5.20	0.2	419	1.27
<i>Ordovician turbidites</i>														
OS31			0.27	−0.24		0.71350	63.4	0.77		5.58	4.54	1.0	186	
OS35			0.02	−0.18		0.71650	56.8	0.76		5.94	5.53	2.2	262	
OS37			−0.53	−0.19		0.71910	89.9	0.29		1.10	1.17	0.3	45	
OS39			−0.55	−0.21		0.71950	80.3	0.51		2.17	2.57	0.2	111	
New England Fold Belt														
<i>New England Batholith</i>														
NEB247	S-type	Bundarra	−0.14	−0.11	12	0.70500	72.7	0.38	2.44		4.32	0.9	193	1.05

Mo isotope composition ($\delta^{98}\text{Mo}$) is relative to NIST SRM3134. Two or more full procedural duplicates were made for each sample analysed. Reproducibility (2s.d.) of all samples is equal or better than $\pm 0.06\text{‰}$.

and assimilation (Halliday et al., 1980). This pluton displays the most primitive isotopic characteristics, with the initial $^{87}\text{Sr}/^{86}\text{Sr}$ and $\delta^{18}\text{O}$ ranging from 0.7041 to 0.7059 and 7.8‰ to 10.3‰, respectively (Halliday et al., 1980).

2.2.2. Criffell

Criffell pluton (397 Ma) comprises a central granite core emplaced into an outer granodiorite (Phillips, 1956). The granodioritic magma is likely to be a hybrid of dioritic magma and metasedimentary melts (Holden et al., 1987). Its petrography is characterised by the common presence of green amphibole and sphene. The subsequently emplaced central granite, which was derived from magma enriched in sediment melt partially mixed in situ with the granodiorite, shows normal concentric zoning becoming more silicic inwards as a result of fractional crystallization (Halliday et al., 1980; Stephens and Halliday, 1980). The granite is marked by the presence of alkali feldspar megacrysts with rare primary muscovite present near the centre. The Criffell pluton displays an initial $^{87}\text{Sr}/^{86}\text{Sr}$ range of 0.7052–0.7069 and $\delta^{18}\text{O}$ of 8.5‰–11.8‰ (Halliday et al., 1980).

2.2.3. Fleet

The Fleet pluton (392 Ma) is composed of an outer coarse-grained biotite granite, a middle coarse-grained biotite-muscovite granite, and a fine-grained biotite-muscovite granite inner core (Parslow, 1968). This pluton displays the smallest petrological diversity with oligoclase and the proportion of biotite/mica ratio decreasing towards the centre. The formation of the structural and petrographic features of Fleet pluton are thought to be caused by multiple intrusion events, magmatic differentiation and post-magmatic processes (Parslow, 1971). The Fleet pluton displays high and variable initial $^{87}\text{Sr}/^{86}\text{Sr}$ ranging from 0.7060 to 0.7109, accompanied by heavy but similar $\delta^{18}\text{O}$ between 11.2‰ and 11.3‰. The derivation of the Fleet pluton may therefore have involved the greatest proportions of sedimentary partial melts (Halliday et al., 1980).

3. METHODS

3.1. Molybdenum isotopes

Fifty-two granitic and four sedimentary samples were analysed for Mo isotopic composition ($\delta^{98}\text{Mo}$) and Mo concentration. Three USGS standards, BHVO-2 (basalt), GSP-2 (granodiorite), G-2 (granite) were analysed as additional samples to provide a long-term monitor of analytical reproducibility. Each batch of analyses included identically processed USGS standards and samples. Samples were weighed, and then double spiked with a known quantity of a ^{97}Mo and ^{100}Mo spike in order to correct for experimental and instrumental Mo isotope fractionation (Siebert et al., 2001). They were then dissolved in Savillex PFA vials by successive acid digestions using HF-HNO₃, HNO₃, and HCl on a hotplate at 90–120 °C. The aliquots for Mo isotope analysis were processed through column

chemistry using anion (Biorad AG1-X8) and cation resin (AG50 W-X8) to guarantee effective separation of Mo from the matrix. The purification method follows that of Wasylenko et al. (2007), however the high Fe/Mo ratio in igneous rocks and the potential isobaric interference of $^{56}\text{Fe}^{40}\text{Ar}$ on ^{96}Mo , required two modifications in order to improve the separation of Mo from Fe: (1) the cation resin separation was processed twice using new resin each time; (2) 30 μl \sim 30% H_2O_2 was added to sample solutions before loading onto the cation resin column. Isotopic compositions were measured on a Nu Instruments multicollector-inductively coupled plasma-mass spectrometer (MC-ICP-MS) in low resolution at the University of Oxford, following the method of Siebert et al. (2001). Molybdenum isotope measurements were made relative to an Alfa Aesar ICP standard solution (Lot 011895D). As NIST SRM3134 has been agreed upon as an international Mo standard (Greber et al., 2012; Goldberg et al., 2013; Nägler et al., 2014), our Mo isotopic composition data are normalized to NIST SRM3134 in order to facilitate inter-laboratory comparison. Data are reported in $\delta^{98}\text{Mo}$ notation expressed as $\delta^{98}\text{Mo} = \left[\left(\frac{^{98}\text{Mo}/^{95}\text{Mo}}{^{98}\text{Mo}/^{95}\text{Mo}} \right)_{\text{sample}} / \left(\frac{^{98}\text{Mo}/^{95}\text{Mo}}{^{98}\text{Mo}/^{95}\text{Mo}} \right)_{\text{standard}} - 1 \right] \times 1000$.

The Oxford Alfar Aesar standard solution used in this study has a $\delta^{98}\text{Mo}$ value of $-0.12 \pm 0.06\text{‰}$ relative to NIST SRM3134 (Greber et al., 2012). In addition, all Mo isotopic compositions cited from the literature in this study have been renormalised to NIST SRM3134, using the values recommended by Goldberg et al. (2013). Full procedural duplicates of the USGS rock standards BHVO-2 ($n = 15$), GSP-2 ($n = 10$), and G-2 ($n = 3$), give an external reproducibility of 0.06‰ (2 s.d.), and yield Mo isotopic compositions of $0.01 \pm 0.06\text{‰}$, $-0.17 \pm 0.06\text{‰}$, and $-0.08 \pm 0.05\text{‰}$, respectively, relative to NIST SRM3134. The $\delta^{98}\text{Mo}$ value of BHVO-2 ($0.01 \pm 0.06\text{‰}$ (2 s.d.) analysed in this study is identical within error to the values reported other studies (e.g. Burkhardt et al., 2014; Li et al., 2014; Zhao et al., 2015). Two to four full procedural duplicates (different aliquots of a sample powder) were made for most samples analysed. Reproducibilities (2 s.d.) of these samples are better than or equal to 0.06‰ .

The concentrations of Mo were determined by isotope dilution MC-ICP-MS using the double spike isotopic composition data. The long-term average Mo concentrations of USGS standards are: BHVO-2 = $3.7 \pm 0.8 \mu\text{g/g}$ (2 s.d., $n = 15$), GSP-2 = $2.1 \pm 0.3 \mu\text{g/g}$ (2 s.d., $n = 15$), and G-2 = $0.23 \pm 0.01 \mu\text{g/g}$ (2 s.d., $n = 3$). The USGS recommended Mo concentration of GSP-2 is $2.1 \pm 0.6 \mu\text{g/g}$; BHVO-2 and G-2 have no [Mo] values recommended by USGS. BHVO-2 shows substantial heterogeneity in Mo content, reflected by the relatively large standard deviation (2 s.d. = $\pm 0.8 \mu\text{g/g}$). This has also been noted by previous studies (Yang et al., 2015; Weis et al., 2005; Burkhardt et al., 2014; Li et al., 2014). The excellent reproducibility of the Mo isotope composition of BHVO-2 ($\pm 0.06\text{‰}$ (2 s.d.)) in this study and the comparison with the data published in the publications above suggest that the Mo isotopic composition of BHVO-2 is unaffected by this inhomogeneity.

3.2. LA-ICP-MS imaging

Two-dimensional elemental images have been acquired via Laser Ablation Inductively Coupled Plasma Mass Spectrometry (LA-ICP-MS) on polished sections of samples DBL-2 and WL10. These analyses were carried out in the LA-ICP-MS lab at GEOMAR Kiel (Germany) using a Nu Instruments ATTOM HR-ICP-MS coupled to a NWR UP193fx excimer laser ablation system equipped with a large format cell (LFC). ICP optimization for robust plasma conditions followed the approach published by Fietzke and Frische (2016) achieving a normalized Argon index NAI of 25–30, resulting in $\text{ThO}/\text{Th} < 0.05\%$. The maximum mass load of material introduced into the plasma did not exceed a matrix Argon index MA of 0.004. Data collection was done in time resolved mode (TRA) as single cycles of 0.22 s integration. During these cycles intensities of the following isotopes have been recorded: ^{23}Al , ^{25}Mg , ^{26}Mg , ^{27}Al , ^{28}Si , ^{29}Si , ^{31}P , ^{34}S , ^{38}Ar , ^{39}K , ^{42}Ca , ^{43}Ca , ^{49}Ti , ^{55}Mn , ^{56}Fe , ^{57}Fe , ^{40}Ar , ^{36}Ar , ^{90}Zr , ^{95}Mo , ^{97}Mo , ^{98}Mo , ^{100}Mo , ^{101}Ru , ^{137}Ba , ^{232}Th , ^{238}U and $^{232}\text{Th}^{16}\text{O}$. Helium (He) was used as ablation cell gas at a flow rate of 0.55 l/min, mixed with Ar (0.53 l/min). Cool gas flow was set to 17.5 l/min, auxiliary gas to 0.56 l/min and the ICP was operated at 1000 W power.

Samples were pre-ablated using line scans at 500 $\mu\text{m/s}$ using 150 μm spots, 60 Hz repetition rate and a laser fluence of 1 J/cm^2 . Analyses of the samples were carried out as a line raster. Each line was 10 mm long, scanned at 50 $\mu\text{m/s}$ using 50 μm spots, 60 Hz repetition rate and a fluence of 3.5 J/cm^2 . Consecutive lines were placed 40 μm apart from each other. Before and after 25 of these lines standards (NIST-SRM610 and USGS BCR-2G) were analysed using spot ablations of 50 μm at 10 Hz to allow for quantification of the images and drift control. Before each ablation pattern (line or spot) the laser warmed up for 10 s and a wash-out delay of 15 s was applied after each individual pattern.

Raw data were first corrected for the average background intensities (gas blank) collected prior to each ablation pattern. The background-corrected intensities were normalized to ^{28}Si for each individual data point, and converted into relative elemental abundances using the measured isotope ^{28}Si and the published concentration values for the two standards. The relative abundances of all elements mentioned above have been integrated for each data point and the proportion of each element relative to this integral has been calculated. The results of 10 mm \times 2 mm sections of both, sample DBL-2 and WL-10, are displayed in Fig. 3.

4. RESULTS

Data for Australian and Scottish samples are presented in Tables 1 and 2, respectively. Analytical uncertainties are represented using the long-term reproducibility $\pm 0.06\%$ (2 s.d.) defined by the USGS rocks standards, BHVO-2, GSP-2 and G-2.

Molybdenum concentrations vary from 0.1 $\mu\text{g/g}$ to 8.1 $\mu\text{g/g}$, with an average of 1.1 $\mu\text{g/g}$, consistent with the

estimated 1.1 $\mu\text{g/g}$ for average continental crust (Rudnick and Gao, 2003), and about the same as that of the LFB sediments (0.9 $\mu\text{g/g}$). None of the sample suites display correlations between [Mo] and magma differentiation indices, such as SiO_2 , K_2O or MgO (not shown); nor does [Mo] correlate with Mo isotopic compositions (Fig. 1a).

The overall whole-rock granitic rocks $\delta^{98}\text{Mo}$ values range from -1.73% to 0.59% , significantly exceeding the variation range of $<1\%$ defined by previously available igneous materials (Siebert et al., 2003; Greber et al., 2011, 2014, 2015; Voegelin et al., 2012, 2014; Yang et al., 2015; Freymuth et al., 2015). The average value of all granitic rocks in this study is $0.09 \pm 0.78\%$ (2 s.d.; $n = 52$). The Mo isotopic compositions of Scottish granitic rocks span a much wider range (-1.73% to 0.45%) than Australia granites (-0.35% to 0.59%) (Fig. 2a), due to the presence of 3 outliers. However, the majority of samples (29 out of 32) define a narrower span ranging from 0% to 0.45% . The LFB sediments exhibit Mo isotope data within the range defined by all granitic rocks (Fig. 2a). Although Mo isotopic compositions of granitic rocks overlap with published basalts (Fig. 2a), the population of the two lithologies clearly differ with granitic rocks dominating heavier $\delta^{98}\text{Mo}$ values (Fig. 2b).

4.1. A-, I- and S-type granites, and sediments from SE Australia

The Mo concentrations of all samples from SE Australia range from 0.1 $\mu\text{g/g}$ to 8.1 $\mu\text{g/g}$ (Table 1). A-type granites show stronger Mo enrichment than both the sediments and the other granite types. The average Mo concentrations for A-, I-, S-type granites and LFB sediments are 3.6 $\mu\text{g/g}$, 0.74 $\mu\text{g/g}$, 1.2 $\mu\text{g/g}$ and 0.93 $\mu\text{g/g}$, respectively. The Mo isotopic composition data of SE Australia granites range from -0.35% to 0.59% , with an average value of $0.08 \pm 0.40\%$ (2 s.d.; $n = 20$). The LFB sediments span a similar but slightly lighter range from -0.56% to 0.27% , averaging $-0.21 \pm 0.70\%$ (2 s.d.; $n = 4$). The Mo isotopic compositions exhibit significant overlaps between differing types of granites, and between granites and sediments (Fig. 2a). Although the A-type granites have slightly heavier Mo isotopic compositions (Fig. 2a), the average values of $\delta^{98}\text{Mo}$ for all granite types from SE Australia are indistinguishable within uncertainty ($\pm 0.06\%$). The S-type sample (NEB247) from the NEB has the lightest Mo isotopic composition (-0.14%) among S-type granites, but still lies within the $\delta^{98}\text{Mo}$ range defined by the other types of LFB granites (Fig. 2a). The $\delta^{98}\text{Mo}$ of granites does not correlate with magmatic differentiation indicators (e.g. SiO_2 , MgO) or with Mo concentration (Fig. 1a,b), although the most Mo-rich sample (AB202, 8.1 $\mu\text{g/g}$) displays the heaviest isotopic signature (0.59%), and the least Mo-enriched sample (MG-58, 0.13 $\mu\text{g/g}$) shows the lightest isotopic composition (-0.35%).

4.2. Granitic rocks from Scotland

The granitic samples from the three plutons (Loch Doon, Criffell, and Fleet) in Scotland have similar Mo

Table 2

Molybdenum isotope and concentration data for granitic rocks from Scotland analysed in this study. Mo isotopic composition ($\delta^{98}\text{Mo}$) is relative to NIST SRM3134. Each $\delta^{98}\text{Mo}$ value represents the average of two to four full procedural duplicates and the reproducibilities of all samples are better than ± 0.06 (2 s.d.). Other isotope data are taken from [Halliday et al. \(1980\)](#).

Sample	Rock type	Locality	$\delta^{98}\text{Mo}$ ‰	$\delta^{30}\text{Si}$ ‰	$\delta^{18}\text{O}$ ‰	$^{87}\text{Sr}/^{86}\text{Sr}(\text{i})$	SiO_2 wt. %	TiO_2 wt. %	Fe_2O_3 (T) wt. %	K_2O wt. %	Mo $\mu\text{g/g}$	Rb $\mu\text{g/g}$	ASI
109	Granodiorite	Criffell	0.29	0.16		0.70533	61.1	0.84	4.70	5.42	0.9	129	0.84
146	Granodiorite	Criffell	0.00	0.15		0.70541	65.8	0.56	3.23	3.39	1.2	126	0.92
243	Granodiorite	Criffell	0.24	0.22	9.05	0.70563	65.1	0.64	3.50	3.63	1.2	140	1.00
244	Granodiorite	Criffell	0.02	0.13	8.54	0.70521	64.4	0.57	3.54	3.96	1.1	120	0.95
184	Granite	Criffell	0.08	0.32		0.70613	67.9	0.48	2.72	4.38	0.8	165	1.07
210	Granite	Criffell	0.21	0.95		0.70683	72.0	0.27	1.77	4.16	0.7	234	1.12
056G	Granite	Criffell	0.33	0.28		0.70602	68.2	0.47	2.61	3.90	1.1		0.96
57–75	Granite	Fleet	0.43	1.11		0.70782	70.7	0.29	1.97	5.65	0.8	279	1.20
58–76	Granite	Fleet	0.45	0.72		0.70667	68.4	0.51	2.86	4.91	0.6	212	1.17
62–68	Granite	Fleet	0.44	1.11		0.70709	72.2	0.28	1.78	5.26	0.4	272	1.11
63–73	Granite	Fleet	0.41	0.88		0.70727	72.4	0.36	2.00	5.00	0.7	250	1.10
60–76	Granite	Fleet	0.22	1.69		0.70955	71.65	0.23	1.48	5.37	1.0	274	1.09
56–72	Granite	Fleet	0.39	1.43	11.33	0.70742	71.4	0.28	1.70	5.50	0.4	301	1.13
56–74	Granite	Fleet	0.39	1.35		0.70747	72.4	0.29	1.78	5.38	0.7	274	1.18
55–69	Granite	Fleet	0.41	3.51		0.70948	73.37	0.13	0.96	5.24	0.9	309	1.20
56–70	Granite	Fleet	0.38	2.55		0.71092	75.65	0.11	0.8	4.86	0.9	310	1.26
57–71	Granite	Fleet	0.34	2.52	11.29	0.70955	73.51	0.16	1.27	4.91	0.8	299	1.19
55–75	Granite	Fleet	−1.73	0.86	11.17	0.70620	69.4	0.53	3.08	4.42	0.5	226	1.03
WL4	Microdiorite	Loch Doon	0.09	0.19		0.70468	59.6	0.85	5.62	3.33	1.3	85	1.06
WL6	Diorite	Loch Doon	0.10	0.10		0.70498	59.1	0.80	6.34	2.59	1.5	73	0.80
WL7	Diorite	Loch Doon	0.20	0.12		0.70501	60.1	0.82	5.96	2.63	1.6	80	0.83
WL8	Diorite	Loch Doon	0.27	0.16		0.70511	61.6	0.84	5.44	2.93	0.7	90	0.87
HH6	Granodiorite	Loch Doon	0.10	0.64		0.70543	70.4	0.41	2.51	4.51	1.5	197	1.02
DBL-2	Granodiorite	Loch Doon	0.14	0.20		0.70521	63.2	0.78	4.71	3.63	2.3	103	0.91
DBL-3	Granodiorite	Loch Doon	0.12	0.22	8.34	0.70525	63.1	0.80	4.87	3.46	1.0	110	0.89
WL9	Granodiorite	Loch Doon	−1.03	0.42		0.70523	67.2	0.59	3.60	3.96	1.4	150	0.96
HH1	Granite	Loch Doon	0.27	0.83		0.70556	71.3	0.34	2.14	4.91	0.5	210	1.13
HH2	Granite	Loch Doon	0.39	0.76		0.70578	71.2	0.28	2.21	4.60	0.5	196	1.10
HH3	Granite	Loch Doon	0.05	0.82	10.23	0.70588	72.1	0.34	2.00	4.65	0.4	202	1.09
HH4	Granite	Loch Doon	0.26	0.84		0.70570	71.6	0.35	2.07	4.75	1.1	214	1.10
HH5	Granite	Loch Doon	0.13	0.70		0.70563	70.3	0.30	2.29	4.59	0.5	202	1.12
WL10	Granite	Loch Doon	−1.15	0.56	10.23	0.70522	68.6	0.49	2.79	4.46	0.7	170	1.00

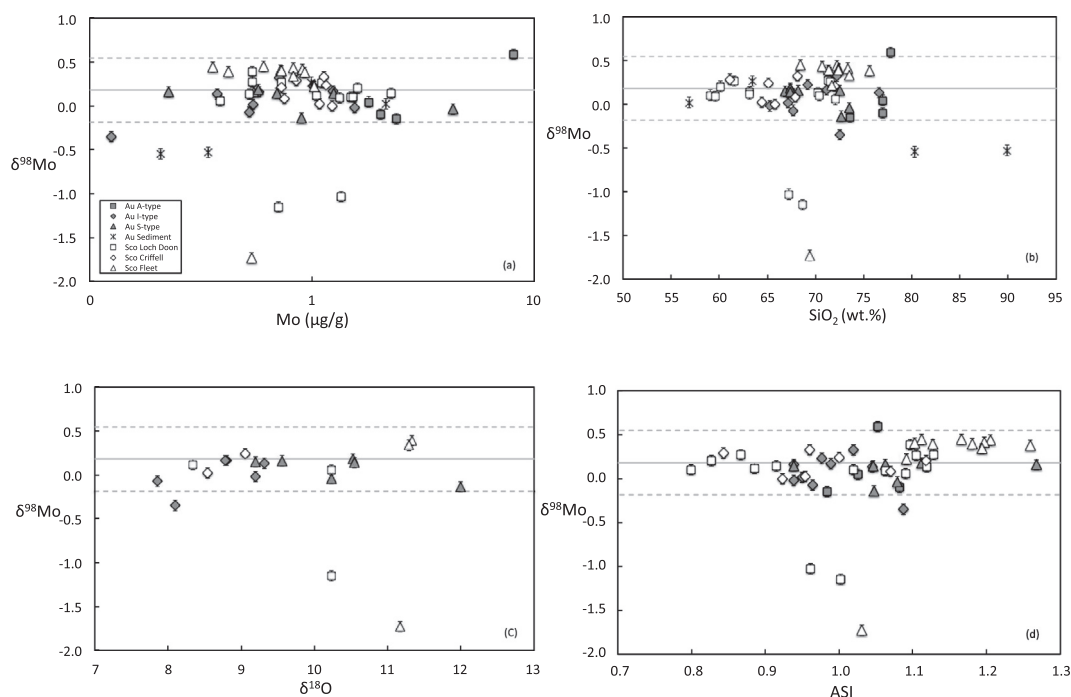


Fig. 1. $\delta^{98}\text{Mo}$ versus (a) Mo concentration, (b) SiO_2 content, (c) $\delta^{18}\text{O}$ (‰), and (d) ASI (Alumina Saturation Index) for granites and sediments from Australia (Au) and for granitic rocks from Scotland (Sco). Error bars are the 2 s.d. of $\pm 0.06\text{‰}$ defined by the long-term reproducibility of USGS standards, BHVO-2, GSP-2 and G-2, and are the same for error bars in all figures of this study. The grey solid lines indicate the mean $\delta^{98}\text{Mo}$ value of the granites excluding the three outliers as shown in the figures. Dashed lines indicate 2 s.d. from the mean.

content ranging from 0.36 to 2.3 $\mu\text{g/g}$, averaging 1.2 $\mu\text{g/g}$, with 1.09 $\mu\text{g/g}$, 0.99 $\mu\text{g/g}$, 0.73 $\mu\text{g/g}$ for Loch Doon, Criffell and Fleet, respectively. The Mo isotopic compositions of Scottish samples range from -1.73‰ to 0.45‰ . The average value of $\delta^{98}\text{Mo}$ for these granitic rocks is $0.10 \pm 0.97\text{‰}$ (2 s.d.; $n = 32$), similar to that of the Australian granites. Excluding the three extreme samples with distinctly negative $\delta^{98}\text{Mo}$ values, the Scottish granitic samples display relatively limited variation in $\delta^{98}\text{Mo}$ from 0‰ to 0.45‰ , with an average of $0.24 \pm 0.28\text{‰}$ (2 s.d.; $n = 29$). Although the Fleet pluton has a greater number of samples towards the heavy end (0.45‰) of the range than Loch Doon and Criffell, the three plutons overlap significantly (Fig. 2a), with average $\delta^{98}\text{Mo}$ of $0.18 \pm 0.20\text{‰}$ (2 s.d.), $0.17 \pm 0.26\text{‰}$ (2 s.d.) and $0.39 \pm 0.13\text{‰}$ (2 s.d.) for Loch Doon, Criffell and Fleet, respectively (outliers excluded). Although there are excellent correlations between SiO_2 and both Rb and Fe_{total} concentration within and between these three plutons, neither Mo concentration nor $\delta^{98}\text{Mo}$ values display correlations with SiO_2 content, suggesting complex behaviour of Mo in granitic systems.

4.3. LA-ICP-MS imaging for DBL-2 and WL10

To explore the underlying mechanism for the extreme $\delta^{98}\text{Mo}$ values of $<-1\text{‰}$ observed in some granitic samples, two samples with contrasting Mo isotopic compositions (DBL-2, 0.14‰ and WL10, -1.15‰) were selected for laser ablation analysis. The results (Fig. 3) show different distributions of Mo in the two samples. In DBL-2, Mo content is

seen to co-vary with Fe, Mg, K and Ti, indicating biotite as the major Mo carrier. In contrast, although biotite is common in WL10 as well, Mo is clearly associated with sulphur content, suggesting Mo is mainly hosted by sulphide in WL10. The distribution of S, Fe, and Mo suggests sulphide occurs in both samples. Investigation of thin sections of the two samples indicates that sulphide presents as secondary pyrite crystals with undetectable Mo in DBL-2, while in WL10, pyrite is not observed but disseminated secondary molybdenite is common. Like biotite, hornblende has also been suggested to accommodate Mo in igneous rocks (Voegelin et al., 2014). Compared to biotite and sulphide, however, hornblende is about 10 times less concentrated in Mo in the two investigated samples, as indicated by relatively low Mo content in areas with high Ca, Mg, Fe. The thin section examination agrees with the LA imaging on mineralogy and fluid alteration is suggested by the overgrowth of sulphide on silicates in both samples and the occasional occurrence of chlorite in WL10.

5. DISCUSSION

5.1. Molybdenum isotopic composition as a source tracer for granitic rocks?

Recent studies have been investigating the potential of stable isotopes of elements such as Si (Savage et al., 2012), Cu (Li et al., 2009), Mg (Li et al., 2010), Li (Teng et al., 2004) and Fe (Foden et al., 2015), as tracers for granite source materials. These elements appear to have

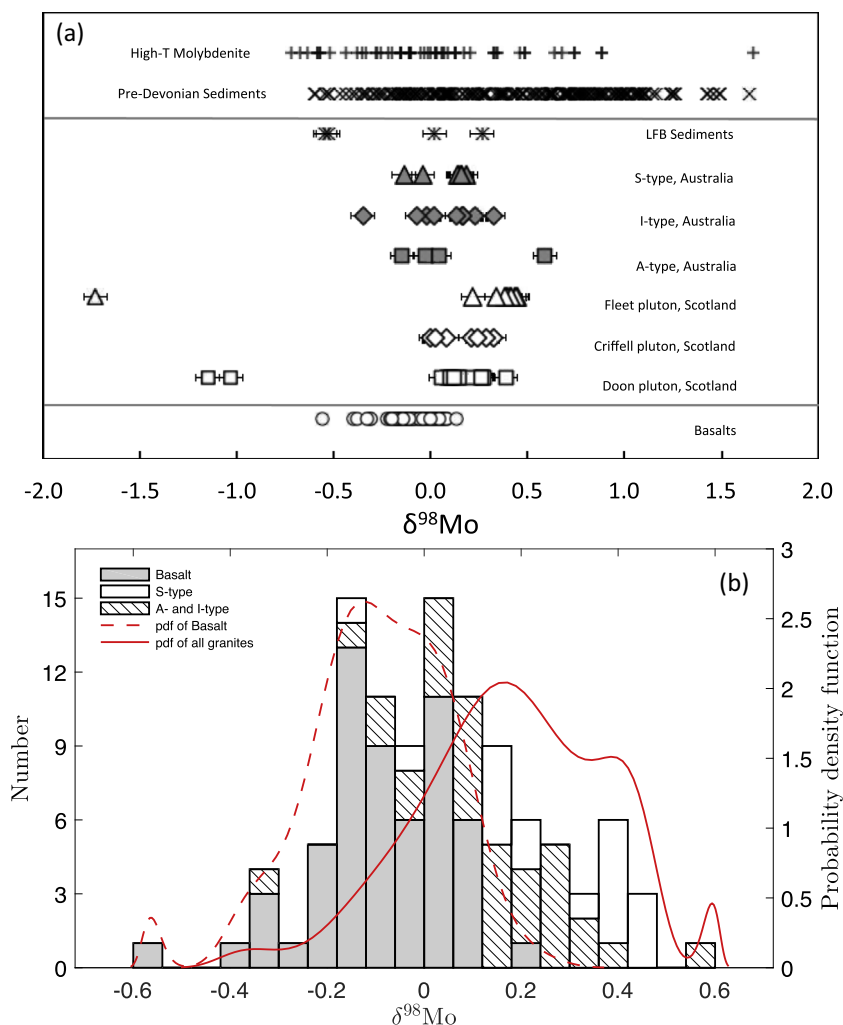


Fig. 2. (a) Molybdenum isotopic composition ($\delta^{98}\text{Mo}$) data for all granitic samples analysed in this study, as well as published pre-Devonian sediments, high-temperature molybdenites, and basalts. Error bars as for Fig. 1. (b) Histogram of $\delta^{98}\text{Mo}$ values with probability density function of A-, I- and S-type granites from this study, excluding three hydrothermally altered samples and published basalts. Sediment data are taken from (Arnold et al., 2004; Siebert et al., 2005; Lehmann et al., 2007; Wille et al., 2007; Kendall et al., 2009, 2011; Duan et al., 2010). Molybdenite data are from (Greber et al., 2014). Data of basalts are taken from (Siebert et al., 2003; Voegelin et al., 2012, 2014; Liang, 2013; Yang et al., 2015; Freymuth et al., 2015).

resolvable differences in their isotopic compositions between granites with different source affinities. In general, isotopic fractionation associated with low-temperature processes is high in comparison to high-temperature processes and therefore is often distinguishable from the latter. In addition, other diagnostic proxies (e.g. $\delta^{18}\text{O}$) for low-T components and interactions can be analysed to support such an interpretation. Low-temperature fingerprints of Si, Cu, Mg, and Li isotopes have indeed been observed in S-types granites. In contrast, the variation of Fe isotopes between different granite types probably results from high temperature magmatic process. Given the significant fractionation of Mo isotopes in low temperature environments recorded in sediments, it is reasonable to assume that granites with sedimentary affinity (S-type) would have a diagnostic range of Mo isotopic compositions reflecting sedimentary source variability, and

Mo isotopes of granitic rocks derived from igneous sources (I- and A-type) would be less variable.

The source material of the analysed S-type granites is thought to be pre-Devonian sediments (e.g. Chappell and Simpson, 1984). Marine sediments older than the Devonian can possess significant variability in Mo isotopic composition ranging from -0.60‰ to 1.64‰ (Fig. 2a) (e.g. Arnold et al., 2004; Siebert et al., 2005; Wille et al., 2007; Kendall et al., 2009, 2011; Duan et al., 2010). However, instead of possessing notable variability or other distinctive features in Mo isotopes, the analysed S-type granites show little difference from I- and A-types with most samples within the isotopic variation defined by I- and A-type granitic rocks (Fig. 2a).

Within the Australian suites, the $\delta^{98}\text{Mo}$ range of S-type granites is bracketed by that of the inferred protolith (LFB

sediments), but they are also overlapping with I- and A-types (Fig. 2a). In the Scottish sample set, anomalously light compositions ($\delta^{98}\text{Mo} < -1\text{‰}$) are present in both I-type (low initial $^{87}\text{Sr}/^{86}\text{Sr}$) and S-type (high initial $^{87}\text{Sr}/^{86}\text{Sr}$) dominated plutons, Loch Doon and Fleet, respectively. Therefore, these extreme compositions are unlikely to relate to any simple source effect, and are more likely to have been caused by some secondary processes as discussed below. Excluding the three outliers, the Fleet pluton ($\delta^{98}\text{Mo} = 0.39 \pm 0.13\text{‰}$ (2 s.d.)), which has S-type affinities, is slightly heavier on average than the Loch Doon ($0.18 \pm 0.20\text{‰}$ (2 s.d.)) and Criffell ($0.17 \pm 0.26\text{‰}$ (2 s.d.)) plutons which have A-/I-type affinities, but the effect is small.

The Australian S-types and the Fleet pluton in Scotland, which is also S-type, have distinct average isotopic compositions ($0.09 \pm 0.25\text{‰}$ and $0.39 \pm 0.13\text{‰}$ respectively). This may indicate the involvement of isotopically different sources in these two regions. However, the ranges of their compositions still partly overlap and the difference between average values is small (Fig. 2a).

The unexpectedly small Mo isotopic variability in S-type granites could imply homogenization of Mo isotopic composition of sediments prior to or during granite genesis, or an efficient mixing process. Alternatively, it could simply indicate that their sources were very close to igneous rocks in Mo isotopic composition, for example, the Mo isotopic composition of LFB Ordovician sediments, which are suggested to be the source of the LFB S-type granites, do overlap with igneous rocks, e.g. basalts, I- and A-type granitic rocks (Fig. 2a).

Overall, unlike other heavy stable isotope systems that have been investigated in granites, Mo isotopic compositions show no systematic distinction between granitic rocks with contrasting source affinities (Fig. 2a). This suggests that Mo isotope fractionation in these rocks reflects different processes from other heavy stable isotope systems and are therefore unlikely to simply discriminate between granite sources.

5.2. Causes of $\delta^{98}\text{Mo}$ variation in granitic rocks

The fractionation of Mo isotopes observed in granitic rocks from SE Australia and Scotland is rather significant for igneous systems. Processes that could affect Mo isotope system in these granitic magmas are discussed below.

5.2.1. Kinetic isotope fractionation by diffusion

It has been proposed that at high temperatures, chemical and thermal diffusion can cause kinetic isotopic fractionation of non-traditional stable isotopes, such as Mg, Fe, and Si (Richter et al., 2008, 2009; Huang et al., 2009, 2010). Experiments have shown that compositional and mineralogical differentiation can occur as a result of thermal diffusion, accompanied by Mg and Fe isotopic fractionation with the enrichment of light isotopes in the hot end (Huang et al., 2009). However, Mg isotopes in LFB granites are not affected by diffusion as they show little deviation from mantle values (Li et al., 2010). Accordingly, it is very unlikely that the higher mass Mo isotopes are affected by such processes.

5.2.2. Secondary alteration: hydrothermal effects

Molybdenum has been demonstrated to have relatively high fluid-melt partition coefficients (D) of 17–20 (e.g. Audétat, 2010), and exsolution of a hydrothermal fluid from a magmatic system is likely accompanied by Mo isotope fractionation (Greber et al., 2011, 2014). In addition, molybdenites precipitated from hydrothermal fluids are seen to have great variability in Mo isotopic composition ranging from -2‰ to 2‰ (Wieser and de Laeter, 2003; Hannah et al., 2007; Malinovsky et al., 2007; Mathur et al., 2010; Greber et al., 2011, 2012; Shafiei et al., 2014). Hence, rock-fluid interaction (such as magmatic-hydrothermal overprint) may alter Mo isotopic composition of affected rock.

Three granitic samples from Scotland, including both I- and S-type samples, have anomalously light Mo isotopic compositions (-1.95‰ to -1.25‰) with no obvious anomalies in available elemental or radiogenic isotope data if compared to the other samples from these plutons. For example, the $\delta^{18}\text{O}$ and the alumina saturation index (ASI) show no significant differences (Table 2). This precludes the possibility of sedimentary assimilation causing such extreme fractionation. Given the $<1\text{‰}$ total variation range in $\delta^{98}\text{Mo}$ defined by available igneous data (see Siebert et al., 2003; Neubert et al., 2011; Voegelin et al., 2012, 2014; Yang et al., 2015; Freymuth et al., 2015), it is unlikely that magmatic processes alone are responsible for the magnitude of isotopic fractionation seen in these three extreme samples. Thus, we propose that their extreme $\delta^{98}\text{Mo}$ values are the result of localized hydrothermal alteration. This is supported by the results of the thin section and LA investigation of sample WL10 (Fig. 3) in which disseminated secondary molybdenite, likely resulting from interaction with Mo-bearing hydrothermal fluid, was observed to be the major Mo carrier. The extremely light Mo isotopic composition seems consistent with isotope values observed during early-stage precipitation of molybdenite (Mo^{4+} -sulphide) from Mo^{6+} dominated aqueous fluids as a result of redox reaction and Rayleigh fractionation (Hannah et al., 2007; Shafiei et al., 2014).

Interestingly, sample DBL-2, with “normal” $\delta^{98}\text{Mo}$ value of 0.14‰ , appears to have been slightly affected by fluid as well, indicated by the occurrence of two secondary pyrite crystals overgrown on silicate minerals (Fig. 3). However, there is no association of Mo with pyrite in DBL-2 and Mo is mostly concentrated in biotite (Fig. 3), suggesting Mo isotopes in DBL-2 is unaffected by fluid infiltration and most likely a primary signal. Because our data strongly suggest hydrothermal overprint as the cause for the extremely negative Mo isotope compositions in the three samples discussed above, we excluded them from the following discussion of igneous effects on Mo isotope compositions and the bulk continental crust.

5.2.3. Igneous processes

Currently available data suggest that Mo is unlikely to be isotopically fractionated during fractional crystallisation of anhydrous phases (Yang et al., 2015), but is fractionated by hydrous phases such as biotite and/or amphibole, as seen in the Kos Plateau Tuff (Aegean Arc) (Voegelin

et al., 2014). A recent study of komatiites (Greber et al., 2015), products of high degrees of partial melting of the mantle, suggests a $\delta^{98}\text{Mo}$ value of -0.21‰ for the bulk silicate earth (BSE) which is lighter than both the average isotopic composition of granitic rocks in this study and the previously suggested $\delta^{98}\text{Mo}$ value for the continental crust (e.g. Voegelin et al., 2014). In addition, published $\delta^{98}\text{Mo}$ values for basalts tend to be lighter than those of granitic rocks (Fig. 2b). Hence, in granitic system igneous melting and differentiation processes have the potential to affect Mo isotopes.

The LA imaging data of samples DBL-2 and WL10 (Fig. 3) confirm earlier suggestions (e.g. Voegelin et al., 2014) that Mo is accommodated by biotite and hornblende in granitic rocks. These two minerals, which are very common crystalline phases in granitic rocks, have been suggested to possess significantly lighter $\delta^{98}\text{Mo}$ compositions than coexisting melt (Voegelin et al., 2014). Therefore, crystallisation and separation of biotite and hornblende may alter the Mo isotopic composition of a given magmatic system. To test whether the presence of hornblende has an effect on the Mo isotope composition of granitic rocks we plotted $\delta^{98}\text{Mo}$ vs. the K/Rb ratio of the granitic samples. Hornblende has been documented to have significantly higher $D^{\text{K/Rb}}$ than other crystalline phases (Philpotts and Schnetzler, 1970; Bernotat et al., 1976) and therefore elevated K/Rb indicates higher proportion of hornblende. As expected from the above, a negative correlation between $\delta^{98}\text{Mo}$ and K/Rb ($R^2 = 0.84$) is observed for LFB I-type granites (Fig. 4a) where hornblende is common (Chappell and White, 2001). The relationship is also present in Scottish samples (Fig. 4b), in which amphibole is common (Gardiner and Reynolds, 1932; Halliday et al., 1980).

A- and S-type granites from Australia show no such correlation, which could simply be due to the absence or rare occurrence of hornblende in these granites (Collins et al., 1982; Chappell and White, 2001).

Molybdenum has been inferred to be able to substitute Fe^{3+} and Ti^{4+} in the lattices of rock-forming minerals due to the observed Mo enrichment in magnetite and ilmenite (e.g. Kuroda and Sandell, 1954). Potential differences in Mo speciation between silicate melt and Fe^{3+} - or Ti^{4+} -rich minerals may result in Mo isotope fractionation. The Mo isotopic composition of I- and S-type granites from Australia, as shown in Fig. 5a and b, does vary substantially with changing $\text{Fe}_2\text{O}_3/\text{TiO}_2$ ratios and Fe_2O_3 content (but not with Ti content (not shown)), particularly in samples with high $\text{Fe}_2\text{O}_3/\text{TiO}_2$, despite the different redox buffers for I-type (IH-HM) and S-type (QFM-MW) magmas indicated by opaque minerals (primarily magnetite and ilmenite) (Chappell and White, 2001, 1992). This observation suggests that magmatic fractionation of Mo isotopes could be associated with preferential uptake of light Mo isotopes by Fe^{3+} -rich minerals and that the oxidation state of magma (at least within the IH-MW buffer) does not affect the behaviour of Mo isotopes. Similar redox independence of Mo isotopes in magmatic systems has also been indicated in Hekla lavas where Mo isotopic compositions were found to be unaffected by potential changes of oxygen and/or sulphur fugacity (Yang et al., 2015). Experimental studies show that Mo occurs predominantly as molybdate species (Mo(VI)) through a wide range of oxygen fugacities (i.e. from air to IW) in both silicate melts and aqueous fluids (Candela and Holland, 1984; Holzheid et al., 1994; Farges et al., 2006a,b; Richter et al., 2016). Hence, the lack of direct redox control on Mo isotopes in these investigated

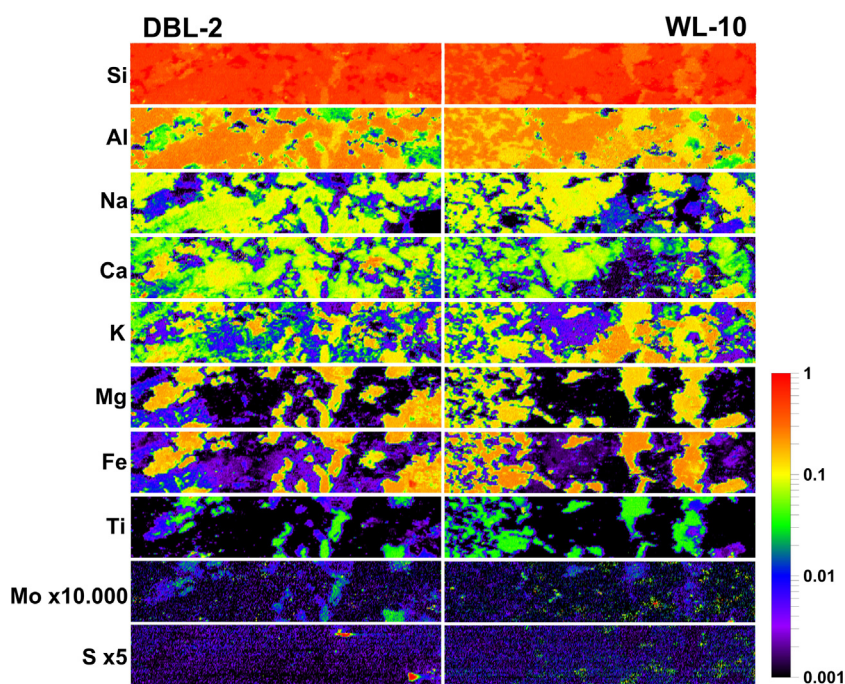


Fig. 3. 2D images ($10\text{ mm} \times 2\text{ mm}$) of the relative abundances of major elements and Mo in samples DBL-2 and WL-10 obtained by LA-ICP-MS. Individual pixel size $11\text{ }\mu\text{m} \times 40\text{ }\mu\text{m}$. Note scaling factor applied on Mo and S data.

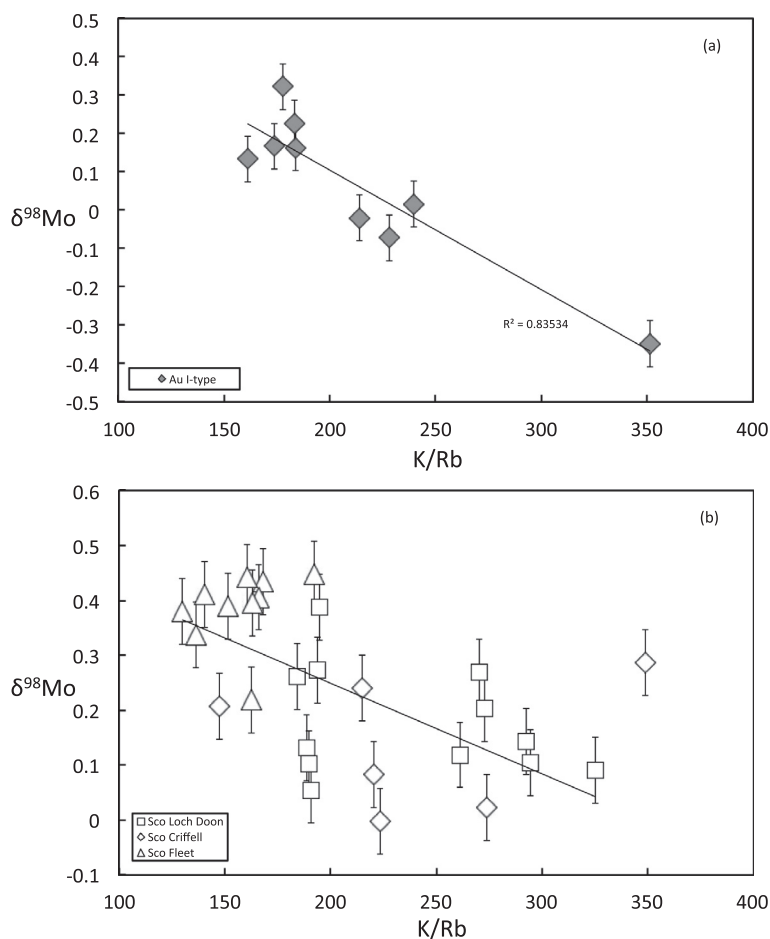


Fig. 4. Plots of $\delta^{98}\text{Mo}$ against K/Rb for (a) I-type granites from Australia and (b) granites from Scotland. Error bars as for Fig. 1.

granitic suites is not surprising. The predominance of tetrahedral Mo(VI) species (unfavourable for crystalline structures) in magma is in accord with its incompatibility during magmatic differentiation (e.g. Voegelin et al., 2014; Yang et al., 2015). This suggests, however, that reduction of Mo valence state and/or changing co-ordination are likely required for Mo to enter the mineral lattice, which would enable fractionation of Mo isotopes, analogous to redox reaction induced isotopic fractionation in low temperature conditions (e.g. Tossell, 2005). Octahedrally coordinated Fe^{3+} in e.g. biotite, hornblende or magnetite has a similar ionic radii to Mo^{4+} or Mo^{3+} (Shannon, 1976) which might explain the observed relationships and the observed preference of Mo for biotite in sample DBL2 and in general for e.g. hornblende and magnetite.

Unlike I- and S-types, the relationship between $\delta^{98}\text{Mo}$ and Fe^{3+} is absent for A-type granites. The Fe_2O_3 content ($[\text{Fe}^{3+}]$) is, on average, significantly lower in A-types (0.58%) than in I-types (1.33%) and S-types (1.03%). Hence the concomitant change in Fe^{3+} content and Mo isotopic composition may be concealed by other factors, which however is difficult to constrain with only 4 data points for A-types. As with the Australian granites, samples from Scotland show no correlation between $\delta^{98}\text{Mo}$ and TiO_2 content. Unfortunately, the effect of Fe^{3+} on Mo isotopes cannot be

assessed for Scottish samples, as the available analyses of these samples do not distinguish between Fe^{3+} and Fe^{2+} oxides.

In summary, our data indicate that, as for iron isotopes (e.g. Foden et al., 2015), petrogenic processes and secondary hydrothermal alteration seem to exert control on the isotopic compositions of Mo in the investigated granitic rocks. However, this assessment is still hampered by the fact that in comparison to Fe, there are few data on Mo behaviour in magmatic systems. Despite this, our data strongly imply that the presence or absence of hydrous minerals/phases and indeed the specific phase present is a controlling factor for the bulk Mo isotope composition of granitic rocks.

5.2.4. Variation of $\delta^{98}\text{Mo}$ in granitic rocks and source heterogeneity

Although the previous discussion showed that Mo isotopic compositions of granitic rocks can be controlled by petrogenic processes, Mo isotopes also systematically vary with Sr isotope composition indicative of source heterogeneity. Surprisingly, I-type granitic samples show variation of Mo isotopes with the initial Sr isotope composition whereas S-type granites are less variable.

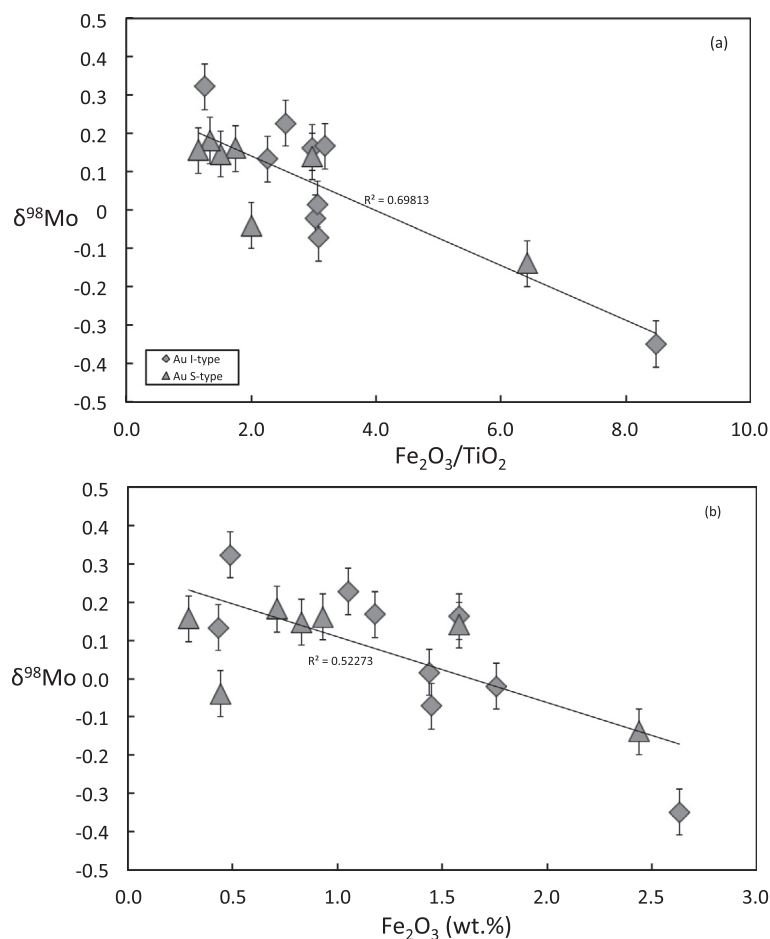


Fig. 5. $\delta^{98}\text{Mo}$ vs. (a) $\text{Fe}_2\text{O}_3/\text{TiO}_2$ ratio and (b) Fe_2O_3 content for I- and S-type granites from Australia. Error bars as for Fig. 1.

Granitic rocks sourced from sediments often have distinctively higher $\delta^{18}\text{O}$ and ASI values than those of igneous origin, as both indices are sensitive to chemical weathering. There are no correlations between $\delta^{98}\text{Mo}$ and $\delta^{18}\text{O}$ or ASI value in the analysed granitic samples (Fig. 1c, d), indicating that the inferred degree of chemical weathering of source materials has little impact on isotopic composition of Mo in granitic rocks.

As shown in Fig. 6, where Mo isotopes are plotted against initial $^{87}\text{Sr}/^{86}\text{Sr}$, Scottish granitic rocks exhibit a distribution curve very similar to but over-arching Australian granites. Both I- and S-type samples from Scotland appear to be heavier in $\delta^{98}\text{Mo}$ than those from SE Australia for a given initial $^{87}\text{Sr}/^{86}\text{Sr}$. This might be suggestive of isotopically distinct regional geology for these granitic rocks.

Interestingly, both Scottish and Australian I-types display positive correlations between Mo isotopes and $^{87}\text{Sr}/^{86}\text{Sr}$ (Fig. 6). This would imply the possibility of mixing between an end member with primitive radiogenic Sr and a light Mo isotopic composition and another with evolved radiogenic Sr and a heavy Mo isotopic composition. Compared to I-types, S-type samples from both locations (except NEB247) are characterised by more radiogenic initial $^{87}\text{Sr}/^{86}\text{Sr}$ (Fig. 6). Nd, Sr and $\delta^{18}\text{O}$ isotopes (Halliday

et al., 1980; Holden et al., 1987) suggest that magmas of the Loch Doon, Criffell and Fleet pluton are mixtures of melts derived by melting of mantle/metabasaltic lower crust, and metasediment (Halliday et al., 1980). Published Mo isotope data for basalts (Siebert et al., 2003; Voegelin et al., 2012, 2014; Liang, 2013; Freymuth et al., 2015; Yang et al., 2015) have an average $\delta^{98}\text{Mo}$ of -0.1‰ , similar to the isotopic compositions of the lightest Scottish I-type sample (Sample 146, $\delta^{98}\text{Mo} = 0\text{‰}$), and such compositions would likely be primitive end members for the Loch Doon and Criffell plutons. The enriched radiogenic Sr source component, identified as metasediments (Halliday et al., 1980), should therefore have a heavy Mo isotopic composition, e.g. reducing sediments (Siebert et al., 2003). Samples from the most radiogenic Sr-enriched Fleet pluton (S-type) are on average heavier than those from the Loch Doon and Criffell pluton (I-type), supporting the greater involvement of sedimentary source components in Fleet among these plutons.

Unlike Scottish samples, the lightest (also the most primitive) LFB I-type granite (MG58) possesses a much lighter Mo isotopic composition of $\delta^{98}\text{Mo} = -0.35\text{‰}$ than basalts, which means that the primitive end member for the LFB I-type granites should be similar to or lighter

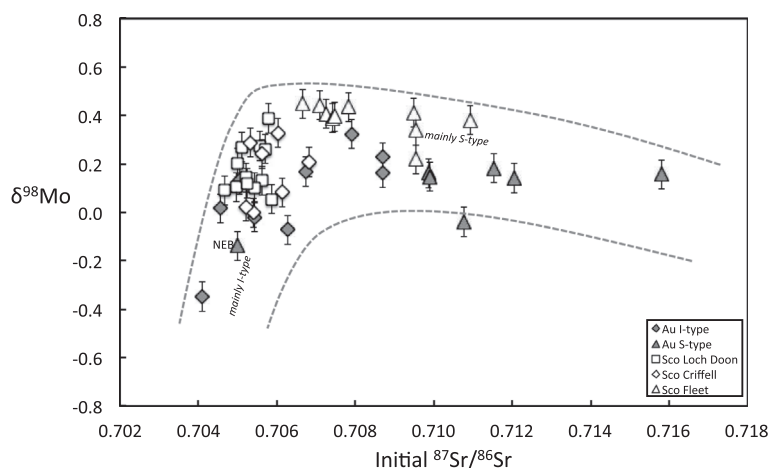


Fig. 6. Plot of $\delta^{98}\text{Mo}$ against initial $^{87}\text{Sr}/^{86}\text{Sr}$ for granites from Australia and Scotland. Dashed lines on top and the bottom follow the distribution patterns of Scottish and Australian granites, respectively. See text for details. Error bars as for Fig. 1.

than this. One possibility is that the source may be subduction related melts, which might preserve light Mo isotope signatures inherited from isotopically light (Siebert et al., 2003) subducted pelagic sediments. However, this hypothesis is hard to reconcile with the evidently low Rb/Nb ratio (5.7), which contrasts with arc magmas related to subduction zones, as such materials would be characterised by elevated large ion lithophile element (LILE) to HFSE ratios (e.g. Ryerson and Watson, 1987, and references therein). In addition, the LFB I-type granites were documented as not compositionally analogous to the granites found in subduction-related continental margins (Chappell et al., 2000). Alternatively, the light Mo isotopic composition could be derived from partial melting of Mo-sulphide-rich basalt with residual/separation of heavy sulphide or an underlying isotopically light lower crustal material from which the I-type granitic rocks might be derived. However, these models need further investigation in the future.

Mixing models suggest that the high $^{87}\text{Sr}/^{86}\text{Sr}$ source component for both I- and S-type granites from LFB could be the Ordovician turbidites (Gray, 1984; Keay et al., 1997). However, high $^{87}\text{Sr}/^{86}\text{Sr}$ sources of I-types are suggested to be mainly pre-existing igneous crust, with only minor/no sedimentary component involved, because the scarcity of inherited zircons combined with the chemical and isotopic data have led to the argument that a sedimentary component is too small to account for the evolved isotopic compositions of radiogenic Sr in the LFB I-type granite (Chappell and White, 1992, 2001; Chappell et al., 1999). It is also unclear from the perspective of Mo isotopes whether high $^{87}\text{Sr}/^{86}\text{Sr}$ LFB I-types are sourced from the same material as LFB S-types. The LFB S-type granites are generally lighter in $\delta^{98}\text{Mo}$ than LFB I-types with evolved radiogenic Sr values (Fig. 6), inconsistent with a common sedimentary source. Hence, the radiogenically enriched Sr source component with heavy Mo isotopic signatures for the LFB I-type granites may be derived from isotopically heavier sedimentary (if any) or granitoid materials.

In contrast to I-type granitic rocks, the overall pattern in Fig. 6 provides evidence that both LFB S-types and the Fleet pluton (S-type) are relatively constant in terms of Mo isotopes, whereas they are much more variable in Sr isotopes. This is unexpected, but might be caused by (1) the lack of variability in Mo isotopes in their particular sedimentary sources, or (2) secondary processes (e.g. hydrothermal, igneous) as discussed above, that averaged out sedimentary source effects. The S-type sample (Sample NEB247) from the NEB shows a regional difference from the LFB S-types by having a lighter Mo isotopic composition and much less evolved initial $^{87}\text{Sr}/^{86}\text{Sr}$, indicating distinct source material.

In summary, the Mo isotope compositions of the investigated granitic rocks are consistent with the interpretations of existing radiogenic isotope data. Molybdenum isotope data appear to be of limited diagnostic value in determining the source of the investigated granitic rocks, however, the data presented here indicate that Mo isotopes in combination with other proxies have the potential to inform on petrogenetic processes. In addition, our data provide a basis for the estimation of the Mo isotope composition of the continental crust and how changing rock formation processes might have influenced this composition in deep time.

5.3. The Mo cycle in the crust

The fifty-two granitic samples analysed in this study increase the igneous data set for Mo isotopic compositions substantially and therefore we attempt to better constrain Mo cycling in the crust.

5.3.1. The Mo isotopic composition of the upper continental crust (UCC)

There are many data for Mo isotopic compositions in sedimentary rocks, particularly reduced sediments (e.g. Scott et al., 2008; Dahl et al., 2010; Duan et al., 2010; Kendall et al., 2011; Herrmann et al., 2012). However, sediments have a wide variety of Mo isotope compositions and

the relative proportion of sediments incorporated in the UCC is variable through time. Therefore, it is difficult to estimate the average Mo isotopic composition of the UCC based on sediments. Unless some portion of isotopically fractionated sediments are removed from the UCC, mass balance in Mo isotopes should constrain the Mo isotopic composition of the weighted average of all sediments to be close to that of the crystalline part of UCC, as all sediments ultimately originated from igneous rocks.

Felsic rocks comprise roughly 50% of the UCC and extend to the middle and lower crust (Wedepohl, 1995). The average Mo isotopic composition of granitic rocks is therefore essential for assessing that of the igneous UCC. The 52 granitic samples in this study, in combination with 6 published granites (Siebert et al., 2003; Greber et al., 2011, 2014; Neubert et al., 2011; Voegelin et al., 2012, 2014), show an unexpectedly large 2.3‰ range in Mo isotopic compositions, but this variability diminishes to 1.0‰ if the three hydrothermally altered samples are eliminated. Granitic rocks, excluding the three outliers, yield an average $\delta^{98}\text{Mo}$ of $0.16 \pm 0.41\text{‰}$ (2 s.d.; $n = 55$). This value represents the average Mo isotopic composition of the felsic portion of the UCC. There is a sizable dataset of Mo isotopes for basalts (Siebert et al., 2003; Voegelin et al., 2012, 2014; Liang, 2013; Yang et al., 2015; Freymuth et al., 2015), which yield an average $\delta^{98}\text{Mo}$ of $-0.10 \pm 0.27\text{‰}$ (2 s.d.; $n = 57$). Given the relatively large sample set for both granitic rocks ($n = 55$) and basalts ($n = 57$) from various localities, the uncertainties of the mean $\delta^{98}\text{Mo}$ values for the two lithologies can be estimated using a 95% standard error of the mean (95% s.e. = $t \times \text{s.d.}/\sqrt{n}$, where t is the inverse survival function of the Student's t -test at the 95% significance level and $n - 1$ degrees of freedom). It reflects the precision of the mean at the 95% confidence level and therefore gives more precise estimates of $\delta^{98}\text{Mo} = 0.16 \pm 0.05\text{‰}$ (95% s.e.) and $\delta^{98}\text{Mo} = -0.10 \pm 0.04\text{‰}$ (95% s.e.) for felsic and basaltic lithologies, respectively. In the absence of Mo isotopic data for metamorphic lithologies, data for granitic rocks, together with those published for basalts, provide the best estimate of $\delta^{98}\text{Mo} = 0.14 \pm 0.07\text{‰}$ (95% s.e. propagated error from the isotopic compositions) for the UCC, comparable to previously estimated values within uncertainty (Greber et al., 2014; Voegelin et al., 2014). This value is derived assuming that the proportion of felsic to basaltic lithologies of the UCC is 10:1 as recommended by Wedepohl (1995).

This UCC value is important for the interpretation of Mo isotopic compositions as an indicator for ocean redox conditions, as well as for the emerging use of Mo isotopes to investigate weathering processes.

5.3.2. Implication for the mass balance of Mo isotopic composition in the crust

As mentioned above, available basaltic rocks define an average $\delta^{98}\text{Mo}$ of $-0.10 \pm 0.04\text{‰}$ (95% s.e.; $n = 57$). Compared to these mantle derived primitive materials, the composition of the UCC represented by granitic rocks is isotopically heavier by more than 0.2‰. This may indicate sequestration of light Mo in the deep crust to give rise to an

isotopically heavier UCC by intracrustal processes. Assuming the Mo isotopic composition of the primordial continental crust is comparable to the average basaltic rocks (-0.1‰), the average lower continental crust (LCC) should have a $\delta^{98}\text{Mo}$ of -0.4‰ to balance out the composition of the UCC of 0.14‰ . This calculation is based on the model of 1:1 upper crust to lower crust (Wedepohl, 1995), and Mo concentration of 0.6 $\mu\text{g/g}$ and 1.1 $\mu\text{g/g}$ for the lower and upper crust respectively (Rudnick and Gao, 2003). However, it is suggested that subducting slabs may preferentially lose heavy Mo during dehydration and fluid release, which would have made the continental crust produced by arc magmatism isotopically heavier than the mantle (Freymuth et al., 2015). This could have lessened the offset between the LCC and UCC in Mo isotopic composition i.e. it could have elevated the $\delta^{98}\text{Mo}$ of the LCC above the calculated value of -0.4‰ .

Possible processes that have the potential to isotopically differentiate the lower and upper continental crust are briefly discussed below.

- (1) Intracrustal igneous processes can produce an isotopically lighter lower crust due to the retention of dense and isotopically light residual hornblende and biotite in the lower crust. Assuming hornblende/biotite are the main phases that accommodate Mo during magmatic differentiation (see above) and using the fractionation factors of $\Delta\delta^{98}\text{Mo}_{\text{hornblende-melt}} = -0.5\text{‰}$ and $\Delta\delta^{98}\text{Mo}_{\text{biotite-melt}} = -0.3\text{‰}$ (Voegelin et al., 2014), a simple Rayleigh model suggest that ~40% of Mo sequestration in the LCC is required to produce an UCC with $\delta^{98}\text{Mo}$ of 0.14‰ by magmatic differentiation. However, the necessary amount of Mo retention in the LCC in this model is too high to be explained by Mo in the two mineral phases alone. Even though Mo has a relatively high partition coefficient in hornblende and biotite with respect to other minerals, it is still incompatible and can only be incorporated in these minerals in trace amounts, i.e. Mo is generally more concentrated in melt than in these minerals. In addition the estimated Mo contents in the UCC (1.1 ppm) and LCC (0.6 ppm) (Rudnick and Gao, 2003) suggest significantly bigger proportion of Mo in the UCC than in the LCC. Hence, other or additional processes are required to account for the isotopic difference between the UCC and LCC.
- (2) High-grade metamorphism could preferentially expel heavy Mo isotopes associated with magmatic sulphides (Voegelin et al., 2012) from the lower crust.
- (3) Subduction of light Mo associated with oxic pelagic sediments could over long timescales enrich the UCC in heavy Mo. Most pelagic sediments will be subducted (Moore, 1975), with only 20% of this subducted sediment reincorporated into continent-building volcanic arcs (Nichols et al., 1994), in contrast to which sediments deposited in often more reducing restricted environments, such as continental margins, may largely escape subduction. The oceans

are thought to have been mostly oxygenated since the Cambrian (e.g. Lyons et al., 2014). This imbalance therefore has the potential to drive the UCC and the Phanerozoic continental crust to heavier Mo isotopic compositions over geological time.

6. CONCLUSIONS

- Although much less variable compared with sedimentary rocks and molybdenite deposits, granitic rocks define a range of 1‰ in Mo isotopic composition, with the $\delta^{98}\text{Mo}$ ranging from -0.41‰ to 0.59‰ . Granitic rocks derived from contrasting source materials show significant overlaps. Hence, the Mo isotopic composition may not be an effective discriminant for distinguishing granites with differing source affinities.
- We suggest the average Mo isotopic composition of the UCC is $0.14 \pm 0.07\text{‰}$, derived from granitic and basaltic rocks.
- The variations of $\delta^{98}\text{Mo}$ in granitic rocks can be induced by multiple factors, including fractional crystallisation, hydrothermal activity, and source heterogeneity. Biotite, hornblende and Fe^{3+} -bearing minerals may be significant repositories for accommodating light Mo isotopes.
- Source mixing models for granitic rocks and mass-balance considerations require the existence of an isotopically lighter lower crust relative to the UCC.

ACKNOWLEDGEMENTS

We are sincerely grateful to the late Bruce W. Chappell for providing Australian granite, sediment samples in support of this study, Nick Belshaw for his help with MC-ICP-MS analysis, Stuart Allison and Colleen J. Bryant for their help with seeking out samples, William McCarthy, Tony Prave, Donald Herd and Peter Cawood for thin section preparation and thought-provoking discussion, and Kuan Xu for his help with MATLAB coding. This manuscript significantly benefits from comments by Craig Lundstrom, Fang Huang, three anonymous reviewers, and the associate editor Frederic Moynier. JY was funded by a Clarendon Scholarship and a Dr Bill Willetts Scholarship from the University of Oxford. The research leading to these results received funding from the European Research Council under the European Union's Seventh Framework Programme (FP7/2007-2013)/ERC grant agreement No. 247422 and from the Science & Technology Facilities Council (STFC Grant number: ST/G00272X/1). The research materials supporting this publication can be accessed by contacting Prof. A.N. Halliday: alex.halliday@earth.ox.ac.uk.

REFERENCES

- Anbar A. D. (2004) Molybdenum stable isotopes: observations, interpretations and directions. *Rev. Mineral. Geochem.* **55**, 429–454. Available at: <http://rimg.geoscienceworld.org/content/55/1/429>.
- Arnold G. L., Anbar A. D., Barling J. and Lyons T. W. (2004) Molybdenum isotope evidence for widespread anoxia in mid-proterozoic Oceans. *Science* **304**(80), 87–90. Available at: <http://www.sciencemag.org/content/304/5667/87>.
- Audétat A. (2010) Source and evolution of molybdenum in the porphyry Mo(–Nb) deposit at cave peak, Texas. *J. Petrol.* **51**, 1739–1760. Available at: <http://petrology.oxfordjournals.org/content/51/8/1739>.
- Barling J., Arnold G. and Anbar A. (2001) Natural mass-dependent variations in the isotopic composition of molybdenum. *Earth Planet. Sci. Lett.* **193**, 447–457. Available at: <http://www.sciencedirect.com/science/article/pii/S0012821X01005143>.
- Bernotat D. W. H., Carron P. J.-P. and Lagache D. M. (1976) K/Rb and Rb/Cs partition between K-feldspars and biotites of pre-Cambrian granites from Sinai. *Tschermaks Mineral. und Petrogr. Mitteilungen* **23**, 23–38. Available at: <http://link.springer.com/article/10.1007/BF01081867>.
- Burkhardt C., Hin R. C., Kleine T. and Bourdon B. (2014) Evidence for Mo isotope fractionation in the solar nebula and during planetary differentiation. *Earth Planet. Sci. Lett.* **391**, 201–211. Available at: <http://www.sciencedirect.com/science/article/pii/S0012821X14000533>.
- Candela P. A. and Holland H. D. (1984) The partitioning of copper and molybdenum between silicate melts and aqueous fluids. *Geochim. Cosmochim. Acta* **48**, 373–380. Available at: <http://www.sciencedirect.com/science/article/pii/0016703784902576>.
- Chappell B. W. and Simpson P. R. (1984) Source rocks of I- and S-type granites in the Lachlan Fold Belt, Southeastern Australia [and Discussion]. *Philos. Trans. R. Soc. London. Ser. A. Math. Phys. Sci.* **310**, 693–707. Available at: <http://rsta.royalsocietypublishing.org/content/310/1514/693.abstract>.
- Chappell B. W. and White A. J. R. (1992) I- and S-type granites in the Lachlan Fold Belt. *Earth Environ. Sci. Trans. R. Soc. Edinburgh* **83**, 1–26. Available at: <http://journals.cambridge.org/action/displayAbstract?fromPage=online&aid=8344777>.
- Chappell B. W. and White A. J. R. (2001) Two contrasting granite types: 25 years later. *Aust. J. Earth Sci.* **48**, 489–499. Available at: <http://onlinelibrary.wiley.com/doi/10.1046/j.1440-0952.2001.00882.x/abstract>.
- Chappell B. W., White A. J. R. and Williams I. S. (1991) A transverse section through granites of the Lachlan Fold Belt. *Aust. Bur. Miner. Resour. Rec.* **22**.
- Chappell B. W., White A. J. R., Williams I. S., Wyborn D., Hergt J. M., Woodhead J. D. and Collins W. J. (1999) Discussion and reply: evaluation of petrogenetic models for Lachlan Fold Belt granitoids: implications for crustal architecture and tectonic models. *Aust. J. Earth Sci.* **46**, 827–836. Available at: <http://www.tandfonline.com/doi/abs/10.1046/j.1440-0952.1999.00742.x>.
- Chappell B. W., White A. J. R., Williams I. S., Wyborn D. and Wyborn L. a. (2000) Lachlan Fold Belt granites revisited: high- and low-temperature granites and their implications. *Aust. J. Earth Sci.* **47**, 123–138. Available at: <http://onlinelibrary.wiley.com/doi/10.1046/j.1440-0952.2000.00766.x/abstract>.
- Collins W. J. (1998) Evaluation of petrogenetic models for Lachlan Fold Belt granitoids: implications for crustal architecture and tectonic models. *Aust. J. Earth Sci.* **45**, 483–500. Available at: <http://www.tandfonline.com/doi/abs/10.1080/08120099808728406>.
- Collins W., Beams S., White A. and Chappell B. (1982) Nature and origin of A-type granites with particular reference to south-eastern Australia. *Contrib. Mineral. Petrol.* **80**, 189–200. Available at: <http://www.springerlink.com/content/pr5562h370215331/abstract/>.
- Dahl T. W., Anbar A. D., Gordon G. W., Rosing M. T., Frei R. and Canfield D. E. (2010) The behavior of molybdenum and its isotopes across the chemocline and in the sediments of sulfidic Lake Cadagno, Switzerland. *Geochim. Cosmochim. Acta* **74**,

- 144–163. Available at: <http://www.sciencedirect.com/science/article/pii/S0016703709005882>.
- Duan Y., Anbar A. D., Arnold G. L., Lyons T. W., Gordon G. W. and Kendall B. (2010) Molybdenum isotope evidence for mild environmental oxygenation before the Great Oxidation Event. *Geochim. Cosmochim. Acta* **74**, 6655–6668. Available at: <http://www.sciencedirect.com/science/article/pii/S0016703710004862>.
- Eby G. N. (1990) The A-type granitoids: a review of their occurrence and chemical characteristics and speculations on their petrogenesis. *Lithos* **26**, 115–134. Available at: <http://www.sciencedirect.com/science/article/pii/002449379090043Z>.
- Farges F., Siewert R., Brown G. E., Guesdon A. and Morin G. (2006a) Structural environments around molybdenum in silicate glasses and melts. I. Influence of composition and oxygen fugacity on the local structure of molybdenum. *Can. Mineral.* **44**, 731–753. Available at: <http://www.canmin.org/content/44/3/731>.
- Farges F., Siewert R., Ponader C. W., Brown G. E., Pichavant M. and Behrens H. (2006b) Structural environments around molybdenum in silicate glasses and melts. II. Effect of temperature, pressure, H₂O. *Halogens and Sulfur. Can. Mineral.* **44**, 755–773. Available at: <http://www.canmin.org/content/44/3/755>.
- Fietzke J. and Frische M. (2016) Experimental evaluation of elemental behavior during LA-ICP-MS: influences of plasma conditions and limits of plasma robustness. *J. Anal. At. Spectrom.* **31**, 234–244. Available at: <http://xlink.rsc.org/?DOI=C5JA00253B>.
- Flood R. H. and Shaw S. E. (1975) A cordierite-bearing granite suite from the New England Batholith, N.S.W., Australia. *Contrib. Mineral. Petrol.* **52**, 157–164. Available at: <http://link.springer.com/10.1007/BF00457291>.
- Foden J., Sossi P. A. and Wawryk C. M. (2015) Fe isotopes and the contrasting petrogenesis of A-, I- and S-type granite. *Lithos* **212**, 32–44. Available at: <http://www.annualreviews.org/doi/abs/10.1146/annurev.earth.28.1.47>.
- Foster D. A. and Gray D. R. (2000) Evolution and structure of the Lachlan Fold Belt (Orogen) of Eastern Australia. *Annu. Rev. Earth Planet. Sci.* **28**, 47–80. Available at: <http://www.annualreviews.org/doi/abs/10.1146/annurev.earth.28.1.47>.
- Freyer H., Vils F., Willbold M., Taylor R. N. and Elliott T. (2015) Molybdenum mobility and isotopic fractionation during subduction at the Mariana arc. *Earth Planet. Sci. Lett.* **432**, 176–186. Available at: <http://www.sciencedirect.com/science/article/pii/S0012821X15006342>.
- Freyer H., Elliott T., van Soest M. and Skora S. (2016) Tracing subducted black shales in the Lesser Antilles arc using molybdenum isotope ratios. *Geology* **44**.
- Frost C. D. and Frost B. R. (2010) On Ferroan (A-type) granitoids: their compositional variability and modes of origin. *J. Petrol.*
- Gardiner C. I. and Reynolds S. H. (1932) The Loch Doon “Granite” Area, Galloway. *Q. J. Geol. Soc.* **88**, 1–NP.
- Goldberg T., Gordon G., Izon G., Archer C., Pearce C. R., McManus J., Anbar A. D. and Rehkämper M. (2013) Resolution of inter-laboratory discrepancies in Mo isotope data: an intercalibration. *J. Anal. At. Spectrom.* **28**, 724–735. Available at: <http://pubs.rsc.org/en/content/articlelanding/2013/ja/c3ja30375f>.
- Gray C. M. (1984) An isotopic mixing model for the origin of granitic rocks in southeastern Australia. *Earth Planet. Sci. Lett.* **70**, 47–60. Available at: <http://www.sciencedirect.com/science/article/pii/0012821X84902085>.
- Gray C. M. (1990) A strontium isotopic traverse across the granitic rocks of southeastern Australia: Petrogenetic and tectonic implications. *Aust. J. Earth Sci.* **37**, 331–349. Available at: <http://www.tandfonline.com/doi/abs/10.1080/08120099008727931>.
- Greber N. D., Hofmann B. A., Voegelin A. R., Villa I. M. and Nägler T. F. (2011) Mo isotope composition in Mo-rich high- and low-T hydrothermal systems from the Swiss Alps. *Geochim. Cosmochim. Acta* **75**, 6600–6609. Available at: <http://www.sciencedirect.com/science/article/pii/S001670371100490X>.
- Greber N. D., Siebert C., Nägler T. F. and Pettke T. (2012) $\Delta 98/95\text{Mo}$ values and Molybdenum Concentration Data for NIST SRM 610, 612 and 3134: towards a Common Protocol for Reporting Mo Data. *Geostand. Geoanal. Res.* **36**, 291–300. Available at: <http://onlinelibrary.wiley.com/doi/10.1111/j.1751-908X.2012.00160.x/abstract>.
- Greber N. D., Pettke T. and Nägler T. F. (2014) Magmatic–hydrothermal molybdenum isotope fractionation and its relevance to the igneous crustal signature. *Lithos* **190–191**, 104–110. Available at: <http://www.sciencedirect.com/science/article/pii/S0024493713003605>.
- Greber N. D., Puchtel I. S., Nägler T. F. and Mezger K. (2015) Komatiites constrain molybdenum isotope composition of the Earth’s mantle. *Earth Planet. Sci. Lett.* **421**, 129–138. Available at: <http://www.sciencedirect.com/science/article/pii/S0012821X15002009>.
- Halliday A. N., Stephens W. E. and Harmon R. S. (1980) Rb–Sr and O isotopic relationships in 3 zoned Caledonian granitic plutons, Southern Uplands, Scotland: evidence for varied sources and hybridization of magmas. *J. Geol. Soc. London* **137**, 329–348. Available at: <http://jgs.lyellcollection.org/content/137/3/329>.
- Hannah J. L., Stein H. J., Wieser M. E., Laeter J. R. and de and Varner M. D. (2007) Molybdenum isotope variations in molybdenite: vapor transport and Rayleigh fractionation of Mo. *Geology* **35**, 703–706. Available at: <http://geology.gsapubs.org/content/35/8/703>.
- Herrmann A. D., Kendall B., Algeo T. J., Gordon G. W., Wasylenko L. E. and Anbar A. D. (2012) Anomalous molybdenum isotope trends in Upper Pennsylvanian euxinic facies: significance for use of $\delta^{98}\text{Mo}$ as a global marine redox proxy. *Chem. Geol.*
- Holden P., Halliday A. N. and Stephens W. E. (1987) Neodymium and strontium isotope content of microdiorite enclaves points to mantle input to granitoid production. *Nature* **330**, 53–56. Available at: <http://www.nature.com/nature/journal/v330/n6143/abs/330053a0.html>.
- Holzheid A., Borisov A. and Palme H. (1994) The effect of oxygen fugacity and temperature on solubilities of nickel, cobalt, and molybdenum in silicate melts. *Geochim. Cosmochim. Acta* **58**, 1975–1981. Available at: <http://www.sciencedirect.com/science/article/pii/0016703794904294>.
- Huang F., Lundstrom C. C., Glessner J., Ianno A., Boudreau A., Li J., Ferré E. C., Marshak S. and DeFrates J. (2009) Chemical and isotopic fractionation of wet andesite in a temperature gradient: experiments and models suggesting a new mechanism of magma differentiation. *Geochim. Cosmochim. Acta* **73**, 729–749. Available at: <http://www.sciencedirect.com/science/article/pii/S0016703708006583>.
- Huang F., Chakraborty P., Lundstrom C. C., Holmden C., Glessner J. J. G., Kieffer S. W. and Lesher C. E. (2010) Isotope fractionation in silicate melts by thermal diffusion. *Nature* **464**, 396–400. Available at: <http://www.nature.com/nature/journal/v464/n7287/full/nature08840.html>.
- Keay S., Collins W. J. and McCulloch M. T. (1997) A three-component Sr–Nd isotopic mixing model for granitoid genesis, Lachlan fold belt, eastern Australia. *Geology* **25**, 307. Available at: <http://adsabs.harvard.edu/abs/1997Geo....25..307K>.
- Kendall B., Creaser R. A., Gordon G. W. and Anbar A. D. (2009) Re–Os and Mo isotope systematics of black shales from the Middle Proterozoic Velkerri and Wollongorang Formations,

- McArthur Basin, northern Australia. *Geochim. Cosmochim. Acta* **73**, 2534–2558. Available at: <http://www.sciencedirect.com/science/article/pii/S0016703709001021>.
- Kendall B., Gordon G. W., Poulton S. W. and Anbar A. D. (2011) Molybdenum isotope constraints on the extent of late Paleoproterozoic ocean euxinia. *Earth Planet. Sci. Lett.* **307**, 450–460. Available at: <http://www.sciencedirect.com/science/article/pii/S0012821X11002901>.
- König S., Wille M., Voegelin A. and Schoenberg R. (2016) Molybdenum isotope systematics in subduction zones.
- Kuroda P. K. and Sandell E. B. (1954) Geochemistry of molybdenum. *Geochim. Cosmochim. Acta* **6**, 35–63. Available at: <http://www.sciencedirect.com/science/article/pii/S0016703754900289>.
- Lehmann B., Nägler T. F., Holland H. D., Wille M., Mao J., Pan J., Ma D. and Dulski P. (2007) Highly metalliferous carbonaceous shale and Early Cambrian seawater. *Geology* **35**, 403–406. Available at: <http://geology.gsapubs.org/content/35/5/403>.
- Leitch E. C. (1974) The geological development of the southern part of the New England Fold Belt. *J. Geol. Soc. Aust.* **21**, 133–156.
- Li W., Jackson S. E., Pearson N. J., Alard O. and Chappell B. W. (2009) The Cu isotopic signature of granites from the Lachlan Fold Belt, SE Australia. *Chem. Geol.* **258**, 38–49. Available at: <http://www.sciencedirect.com/science/article/pii/S000925410800260X>.
- Li W.-Y., Teng F.-Z., Ke S., Rudnick R. L., Gao S., Wu F.-Y. and Chappell B. W. (2010) Heterogeneous magnesium isotopic composition of the upper continental crust. *Geochim. Cosmochim. Acta* **74**, 6867–6884. Available at: <http://www.sciencedirect.com/science/article/pii/S0016703710004795>.
- Li J., Liang X.-R., Zhong L.-F., Wang X.-C., Ren Z.-Y., Sun S.-L., Zhang Z.-F. and Xu J.-F. (2014) Measurement of the isotopic composition of molybdenum in geological samples by MC-ICP-MS using a novel chromatographic extraction technique. *Geostand. Geoanal. Res.* **38**, 345–354. Available at: <http://onlinelibrary.wiley.com/doi/10.1111/j.1751-908X.2013.00279.x/abstract>.
- Liang Y.-H. (2013) Mass dependent isotopic fractionation of molybdenum in the solar system.
- Loiselle M. C. and Wones D. R. (1979) Characteristics and origin of anorogenic granites. *Geol. Soc. Am. Abstr. Programs* **11**, 468.
- Lyons T. W., Reinhard C. T. and Planavsky N. J. (2014) The rise of oxygen in Earth's early ocean and atmosphere. *Nature* **506**, 307–315. Available at: <http://www.nature.com/nature/journal/v506/n7488/full/nature13068.html>.
- Malinovsky D., Hammarlund D., Ilyashuk B., Martinsson O. and Gelting J. (2007) Variations in the isotopic composition of molybdenum in freshwater lake systems. *Chem. Geol.* **236**, 181–198. Available at: <http://www.sciencedirect.com/science/article/pii/S000925410600427X>.
- Mathur R., Brantley S., Anbar A., Munizaga F., Maksiyev V., Newberry R., Vervoort J. and Hart G. (2010) Variation of Mo isotopes from molybdenite in high-temperature hydrothermal ore deposits. *Miner. Depos.* **45**, 43–50. Available at: <http://www.springerlink.com/content/157q336157257215/abstract/>.
- McCulloch M. T. and Chappell B. W. (1982) Nd isotopic characteristics of S- and I-type granites. *Earth Planet. Sci. Lett.* **58**, 51–64. Available at: <http://adsabs.harvard.edu/abs/1982E%2526PSL...58...51M>.
- McCulloch M. and Woodhead J. (1993) Lead isotopic evidence for deep crustal-scale fluid transport during granite petrogenesis. *Geochim. Cosmochim. Acta* **57**, 659–674. Available at: <http://adsabs.harvard.edu/abs/1993GeCoA...57..659M>.
- Mensel H., McCulloch M. and Chappell B. (1985) The New England Batholith: constraints on its derivation from Nd and Sr isotopic studies of granitoids and country rocks. *Geochim. Cosmochim. Acta* **49**, 369–384. Available at: <http://adsabs.harvard.edu/abs/1985GeCoA...49..369M>.
- Moore J. C. (1975) Selective subduction. *Geology* **3**, 530–532.
- Nägler T. F., Anbar A. D., Archer C., Goldberg T., Gordon G. W., Greber N. D., Siebert C., Sohrin Y. and Vance D. (2014) Proposal for an international molybdenum isotope measurement standard and data representation. *Geostand. Geoanal. Res.* **38**, 149–151.
- Neubert N., Heri A. R., Voegelin A. R., Nägler T. F., Schlunegger F. and Villa I. M. (2011) The molybdenum isotopic composition in river water: constraints from small catchments. *Earth Planet. Sci. Lett.* **304**, 180–190.
- Nichols G. T., Wyllie P. J. and Stern C. R. (1994) Subduction zone melting of pelagic sediments constrained by melting experiments. *Nature* **371**, 785–788.
- O'Neil J. R. and Chappell B. W. (1977) Oxygen and hydrogen isotope relations in the Berridale batholith. *J. Geol. Soc. London* **133**, 559–571. Available at: <http://jgs.lyellcollection.org/content/133/6/559.abstract>.
- O'Neil J. R., Shaw S. E. and Flood R. H. (1977) Oxygen and hydrogen isotope compositions as indicators of granite genesis in the New England Batholith. *Australia. Contrib. to Mineral. Petrol.* **62**, 313–328. Available at: <http://link.springer.com/article/10.1007/BF00371018>.
- Parslow G. R. (1968) The physical and structural features of the Cairnmore of Fleet granite and its aureole. *Scottish J. Geol.* **4**, 91–108.
- Parslow G. R. (1971) Variations in mineralogy and major elements in the Cairnmore of Fleet granite, S.W., Scotland. *Lithos* **4**, 43–55.
- Phillips W. J. (1956) The Criffell-Dalbeattie granodiorite complex. *Q. J. Geol. Soc.* **112**, 221–239.
- Philpotts J. A. and Schnetzler C. C. (1970) Phenocryst-matrix partition coefficients for K, Rb, Sr and Ba, with applications to anorthosite and basalt genesis. *Geochim. Cosmochim. Acta* **34**, 307–322.
- Planavsky N. J., Asael D., Hofmann A., Reinhard C. T., Lalonde S. V., Knudsen A., Wang X., Ossa Ossa F., Pecoits E., Smith A. J. B., Beukes N. J., Bekker A., Johnson T. M., Konhauser K. O., Lyons T. W. and Rouxel O. J. (2014) Evidence for oxygenic photosynthesis half a billion years before the Great Oxidation Event. *Nat. Geosci.* **7**, 283–286.
- Richter F. M., Watson E. B., Mendybaev R. A., Teng F.-Z. and Janney P. E. (2008) Magnesium isotope fractionation in silicate melts by chemical and thermal diffusion. *Geochim. Cosmochim. Acta* **72**, 206–220.
- Richter F. M., Dauphas N. and Teng F.-Z. (2009) Non-traditional fractionation of non-traditional isotopes: evaporation, chemical diffusion and Soret diffusion. *Chem. Geol.* **258**, 92–103.
- Righter K., Danielson L. R., Pando K. M., Shofner G. A., Sutton S. R., Newville M. and Lee C.-T. (2016) Valence and metal/silicate partitioning of Mo: implications for conditions of Earth accretion and core formation.
- Rudnick R. L. and Gao S. (2003) 3.01 – Composition of the Continental Crust. In (eds. Editors-in-Chief: Heinrich D. Holland and Karl K. Turekian). Pergamon, Oxford. pp. 1–64.
- Ryerson F. J. and Watson E. B. (1987) Rutile saturation in magmas: implications for TiNbTa depletion in island-arc basalts. *Earth Planet. Sci. Lett.* **86**, 225–239.
- Savage P. S., Georg R. B., Williams H. M., Turner S., Halliday A. N. and Chappell B. W. (2012) The silicon isotope composition of granites. *Geochim. Cosmochim. Acta* **92**, 184–202.

- Scott C., Lyons T. W., Bekker A., Shen Y., Poulton S. W., Chu X. and Anbar A. D. (2008) Tracing the stepwise oxygenation of the Proterozoic ocean. *Nature* **452**, 456–459.
- Shafiei B., Shalamanian G., Mathur R. and Mirnejad H. (2014) Mo isotope fractionation during hydrothermal evolution of porphyry Cu systems. *Miner. Depos.* **50**, 281–291.
- Shand S. J. (1927) On the Relations between Silica, Alumina, and the Bases in Eruptive Rocks, considered as a Means of Classification. *Geol. Mag.* **64**, 446–449.
- Shannon R. D. (1976) Revised effective ionic radii and systematic studies of interatomic distances in halides and chalcogenides. *Acta Crystallogr. Sect. A* **32**, 751–767.
- Shaw S. E. and Flood R. H. (1981) The New England Batholith, Eastern Australia: geochemical variations in time and space. *J. Geophys. Res.* **86**(10530–10), 544.
- Siebert C., Nögler T. F. and Kramers J. D. (2001) Determination of molybdenum isotope fractionation by double-spike multicollector inductively coupled plasma mass spectrometry. *Geochemistry Geophys. Geosystems* **2**, 1032–1116. Available at: <http://www.agu.org/pubs/crossref/2001/2000GC000124.shtml>.
- Siebert C., Nögler T. F., von Blanckenburg F. and Kramers J. D. (2003) Molybdenum isotope records as a potential new proxy for paleoceanography. *Earth Planet. Sci. Lett.* **211**, 159–171.
- Siebert C., Kramers J. D., Meisel T., Morel P. and Nögler T. F. (2005) PGE, Re–Os, and Mo isotope systematics in Archean and early Proterozoic sedimentary systems as proxies for redox conditions of the early Earth. *Geochim. Cosmochim. Acta* **69**, 1787–1801.
- Stephens W. E. and Halliday A. N. (1980) Discontinuities in the composition surface of a zoned pluton, Criffell. *Scotland. Geol. Soc. Am. Bull.* **91**, 165–170.
- Teng F.-Z., McDonough W. F., Rudnick R. L., Dalpé C., Tomascak P. B., Chappell B. W. and Gao S. (2004) Lithium isotopic composition and concentration of the upper continental crust. *Geochim. Cosmochim. Acta* **68**, 4167–4178.
- Tindle A. G. and Pearce J. A. (1981) Petrogenetic modelling of in situ fractional crystallization in the zoned Loch Doon pluton, Scotland. *Contrib. Mineral. Petrol.* **78**, 196–207.
- Tossell J. A. (2005) Calculating the partitioning of the isotopes of Mo between oxidic and sulfidic species in aqueous solution. *Geochim. Cosmochim. Acta* **69**, 2981–2993.
- Voegelin A. R., Nögler T. F., Pettke T., Neubert N., Steinmann M., Pourret O. and Villa I. M. (2012) The impact of igneous bedrock weathering on the Mo isotopic composition of stream waters: natural samples and laboratory experiments. *Geochim. Cosmochim. Acta* **86**, 150–165.
- Voegelin A. R., Pettke T., Greber N. D., von Niederhäusern B. and Nögler T. F. (2014) Magma differentiation fractionates Mo isotope ratios: evidence from the Kos Plateau Tuff (Aegean Arc). *Lithos* **190–191**, 440–448.
- Wasylenki L. E., Anbar A. D., Liermann L. J., Mathur R., Gordon G. W. and Brantley S. L. (2007) Isotope fractionation during microbial metal uptake measured by MC-ICP-MS. *J. Anal. At. Spectrom.* **22**, 905–910.
- Wedepohl P. D. K. H. (1991) Chemical composition and fractionation of the continental crust. *Geol. Rundschau* **80**, 207–223. Available at: <http://link.springer.com/article/10.1007/BF01829361>.
- Wedepohl K. (1995) The composition of the continental crust. *Geochim. Cosmochim. Acta* **59**, 1217–1232.
- Weis D., Kieffer B., Maerschalk C., Pretorius W. and Barling J. (2005) High-precision Pb–Sr–Nd–Hf isotopic characterization of USGS BHVO-1 and BHVO-2 reference materials. *Geochem., Geophys. Geosyst.* **6**, Q02002.
- Whalen J. B., Currie K. L. and Chappell B. W. (1987) A-type granites: geochemical characteristics, discrimination and petrogenesis. *Contrib. Mineral. Petrol.* **95**, 407–419.
- White A. J. R., Williams I. S. and Chappell B. W. (1976) The Jindabyne Thrust and its Tectonic, physiographic and petrogenetic significance. *J. Geol. Soc. Aust.* **23**, 105–112.
- Wieser M. E. and de Laeter J. R. (2003) A preliminary study of isotope fractionation in molybdenites. *Int. J. Mass Spectrom.* **225**, 177–183.
- Wille M., Kramers J. D., Nögler T. F., Beukes N. J., Schröder S., Meisel T., Lacassie J. P. and Voegelin A. R. (2007) Evidence for a gradual rise of oxygen between 2.6 and 2.5 Ga from Mo isotopes and Re–PGE signatures in shales. *Geochim. Cosmochim. Acta* **71**, 2417–2435.
- Wyborn L. A. I. and Chappell B. W. (1983) Chemistry of the Ordovician and Silurian greywackes of the Snowy Mountains, southeastern Australia: an example of chemical evolution of sediments with time. *Chem. Geol.* **39**, 81–92.
- Yang J., Siebert C., Barling J., Savage P., Liang Y.-H. and Halliday A. N. (2015) Absence of molybdenum isotope fractionation during magmatic differentiation at Hekla volcano, Iceland. *Geochim. Cosmochim. Acta* **162**, 126–136.
- Zhao P.-P., Li J., Zhang L., Wang Z.-B., Kong D.-X., Ma J.-L., Wei G.-J. and Xu J.-F. (2015) Molybdenum mass fractions and isotopic compositions of international geological reference materials. *Geostand. Geoanal. Res.*. Available at: <http://doi.wiley.com/10.1111/j.1751-908X.2015.00373.x>.

Associate editor: Frederic Moynier